Technische Universität München

Physik Department E13

Aggregation behavior of water-soluble amphiphilic block copolymers

Tune Bjarke Bonné

Vollständiger Abdruck der von der Fakultät für Physik
der Technischen Universität München zur Erlangung
des akademischen Grades eines

Doktors der Naturwissenschaften

genehmigten Dissertation.

Vorsitzender: Univ.-Prof. Dr. R. Netz

Prüfer der Dissertation:

1. Univ.-Prof. Dr. Chr. Papadakis
2. Univ.-Prof. Dr. M. Rief

Die Dissertation wurde am 15.11.2005 bei der Technischen Universität München eingereicht und durch die Fakultät für Physik am 11.01.2006 angenommen.

Abstract

English abstract

Polymers and block copolymers based on 2-alkyl-2-oxazoline have the advantage that their hydrophobicity can be varied by changing the length of the alkyl side chain and that fluorescence groups can be attached to the block ends. We have studied the aggregation behavior of 2-alkyl-2-oxazoline based diblock, triblock and random copolymers in aqueous solutions, using fluorescence correlation spectroscopy (FCS), where fluorescence labeled polymers were used as tracers. FCS experiments in combination with PCS and SANS were used to investigate the aggregation behavior, with focus on the unimer-micelle transition.

German abstract

Polymere und Blockcopolymere auf der Basis von 2-Alkyl-2-Oxazolin weisen den Vorteil auf, dass ihre Hydrophobizität durch eine Längenänderung der Alkylseitenkette variiert werden kann, bzw. dass die Blockenden mit Fluroeszenzgruppen funktionalisiert werden können. In der vorliegenden Arbeit wird das Aggregationsverhalten von solchen Diblock-, Triblock- und statistischen Copolymeren in wässriger Lösung beschrieben. Die Fluoreszenzkorrelationsspektroskopie wurde für Tracerdiffusionsexperimente fluoreszenzmarkierter Polymere durchgeführt. In Kombination mit Photonenkorrelationsspektroskopie und Neutronenkleinwinkelstreuung wurde insbesondere der Übergang von Unimeren zu Mizellen charakterisiert.

Preface

The present report is the result of a Ph.D.-work, which was started in October 2001 at the Institute of Experimental Physics I, university of Leipzig, under the supervision of Prof. Dr. Christine Papadakis. Polymer samples were supplied from Thomas Komenda, Karin Lüdtke and Dr. Rainer Jordan from the Chemistry Department, TU München. Fluorescence correlation spectroscopy experiments were carried out at the Faculty of Biosciences, Pharmacy and Psychology, University of Leipzig. I spent April - July 2003, as well as December 2003 at the Institute of Macromolecular Chemistry, Academy of Sciences of the Czech republic, Prague, where I performed photon correlation spectroscopy measurements.

In February 2004, we moved to the Physics Department of the Technical University of München, where the project was continued. The fluorescence correlation spectroscopy measurements were performed at the Center for NanoScience, Ludwig-Maximilians-Universität, München.

Acknowledgements

Many people have been very helpful while I have been working on this project and without their help, it would never have been possible.

Firstly I would like to thank my supervisor Prof. Dr. Christine Papadakis, who was courageous enough to invite me abroad and let me work at this project.

Karin Lüdtke, Thomas Komenda and Dr. Rainer Jordan from the Chemistry department at TU München, for good collaboration.

Dr. Petr Štěpánek at the Institute of Macromolecular Chemistry, Academy of Sciences of the Czech Republic in Prague, for inviting me to perform PCS for a total of four months in his laboratory. I would also like to thanks Dr. Jaroslav Holoubek and Dr. Čestmír Koňák for many enlightening discussions.

Prof. Dr. Friedrich Kremer and his group PAF (Physik Anisotroper Fluide), at the Institute of Experimental Physics I, University of Leipzig, for allowing me work in the group and making me feel welcome.

Prof. Dr. Joachim Rädler, Simon Keller and Johannes Bayer, Center for NanoScience, Ludwig-Maximilians-Universität München, for the possibility to perform fluorescence correlation spectroscopy.

Dr. Thomas Greiner-Stöffele and Prof. Dr. Ulrich Hahn, Faculty of Biology, Pharmacy and Psychology, University of Leipzig, for introduction to and use of fluorescence correlation spectroscopy.

The group E13 at the Physics Department at TU München, for making me feel welcome here and showing me that there are other things in Bayern than the university.

I would also gratefully acknowledge financial support by the Deutsche Forschungsgemeinschaft and the European Union's Marie Curie Training Site Program.

Last, but certainly not least, I would like to send a kind thought to my family and friends, just for being who they are (keep up the good work). None mentioned, none forgotten!

Contents

1 Introduction

The self-assembly of amphiphilic (molecules with both a hydrophilic and hydrophobic part) is of great importance for biological systems and technical purposes [1]. In biological systems, self-assembly is observed in e.g. membranes, where lipids form bilayers which is the structure of biological membranes [1]. Also protein aggregation has received a lot of attention, due to their role in various diseases, such as Alzheimer and Creutzfeldt-Jakob disease [2, 3].

Synthetic amphiphilic block copolymers also form aggregates in solutions, where the solvent is selective to one block. This has been used widely in industrial applications, such as detergents, dispersion stabilization, foaming, emulsification, lubrication and formulation of cosmetics and inks [4].

In recent years, both practical and theoretical aspects of the aggregation behavior of block copolymers have been investigated [5, 6, 7, 8, 9, 10, 11, 12]. Some different polymer architectures are shown in figure 1.1. The most

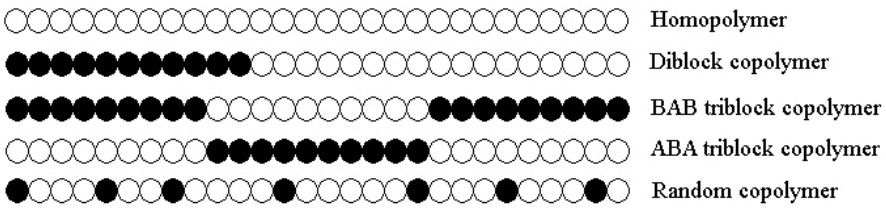

Figure 1.1 Different architectures of polymers. Open circles and closed circles symbolize the hydrophilic (A) and the hydrophobic groups (B), respectively.

simple structure is the homopolymer, where all the monomer units are the same (not necessarily hydrophilic monomers as shown in figure 1.1). Diblock copolymers consist of two blocks with different monomers. If diblock copolymers are dissolved in a selective solvent that is a good solvent for one block and a bad solvent for the other, these polymers can form micelles, if the concentration is above the critical micelle concentration (CMC) [4]. The CMC is

the concentration, where micelles (or aggregates) are formed and below this concentration, the polymers are present as unimers [13], as sketched in figure 1.2. The micelles consist of a core of the insoluble block and a corona formed by the soluble block. ABA type triblock copolymers (where A and B denotes the soluble and insoluble block, respectively) can also form micelles in solution. For these triblock copolymers the middle block forms the core of the micelle, whereas the end blocks forms the corona [4]. The BAB type triblock copolymers, where the middle block is soluble, can also form aggregates, but these are different than for the ABA triblock copolymer aggregates. There is the possibility that the two end blocks are part of the same micelle, so that the middle block forms a loop (a so-called flower micelle), or there is the possibility that the end blocks are part of two different micelles whereby larger aggregates are formed (so-called animals) [14, 15, 16]. The last polymer architecture shown in figure 1.1 is the random or statistical copolymer. For this type of copolymers, the different monomer units are not ordered in blocks, but are distributed randomly along the polymer chain. These types of polymers form aggregates, but they cannot form core-shell aggregates like the block copolymers and is has been suggested that they form aggregates with more hydrophobic domains [17].

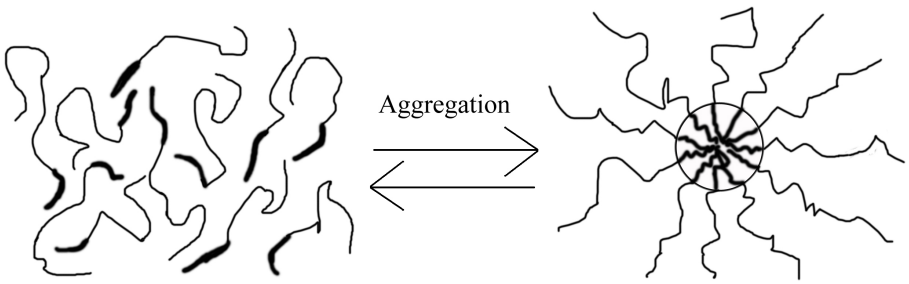

Figure 1.2 Sketch of micelle formation in aqueous solution. Unimers from block copolymers (left) aggregate and form a micelle (right). The thick line symbolizes the hydrophobic part. The micelle sketched here is a core-shell micelle, where the core is made from the hydrophobic block and is surrounded by a shell of the hydrophilic block.

Because of the structure of the micelles, where a part is poorly soluble in the solvent, many investigations have focussed on applications, where otherwise insoluble particles are dissolved in the micellar core. For example cleaning of waste water, where contaminants that are poorly soluble in water will preferential be present in the micellar core and the micelles can be removed by extraction [18]. Another application is drug delivery, where the drug is

dissolved in the micellar core and will be released under specific conditions, depending on the nature of the drug [19, 20, 21]. Block copolymer micelles have also been functionalized for specific purposes, as for example nano-reactors where chemical reactions take place locally in the micellar core [22, 23].

Numerous methods have been applied to investigate the aggregation behavior of different block copolymer systems, e.g. dynamic scanning calorimetry [24], electron microscopy [25], small angle neutron [26] and X-ray scattering [27], photon correlation spectroscopy [28], static light scattering [29, 30], pulsed field gradient NMR [31, 32], dynamic mechanical spectroscopy [33, 34] and surface tension measurements [24]. In this way, the following parameters have been determined for different polymer systems [35]:

- The equilibrium constant for the equilibrium between micelles and unimers
- The critical micelle concentration (CMC) and the critical micelle temperature (CMT)
- The molar mass of the micelles, M_n
- The aggregation number (or association number), N_{agg}, e.g. the average number of unimers in a micelle
- The morphology and structure of the aggregates
- The radius of gyration of a micelle, r_g
- The hydrodynamic radius, r_H, and the diffusion coefficient, D, of the micelle
- The micellar core radius, r_c (see figure 1.3)
- The thickness of the micelle corona (shell), L_c, formed by the soluble blocks (see figure 1.3)

The aggregation of block copolymers are often described by the closed association model [1, 13]. In this model, the association of polymers is assumed to be an equilibrium between unimers and micelles with a dominating aggregation number, N_{agg}. The structure of the micelles have been modelled using mean-field lattice theory, using a spherical lattice (the micelles are assumed to be spherical) where all lattice sites have equal volume and are equidistant [36]. The interaction parameters between the polymer blocks and the

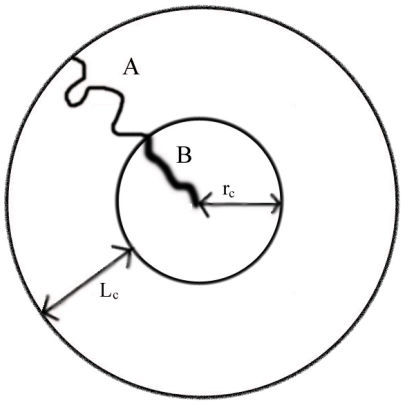

Figure 1.3 Sketch of a spherical micelle, which shows the core radius (r_c) from the B block and corona thickness (L_c) from the A block.

solvent, as well as the interaction parameter between the A and B block, plays an important role. Linse [37] modelled the aggregates of the Pluronics system (a triblock copolymer with propylene oxide as the middle block and ethylene oxide for the end-blocks). The interaction parameters between the blocks and the solvent were determined by a fit to the experimental phase diagrams for the homopolymers. The interaction parameters between the two blocks, were determined by a fit to the phase diagram of mixtures of the two homopolymers and water at two different temperatures [38]. In this manner, Linse was able to predict aggregation properties in aqueous solution for a large Pluronics polymer [37].

Formation of equilibrium micelles are not always achieved by dissolving the polymer in a selective solvent [35, 39]. Reaching equilibrium may be very slow, especially if the hydrophobic (in aqueous solution) part is very insoluble or is in a glassy or crystalline state. Micellar solutions are therefore often prepared by one of the two following procedures [35]; (i) The polymer is dissolved in a solvent, that is a good solvent for both blocks. After this, the selectivity of the solvent is changed, such that micelle formation is required (changing solvent composition or temperature). Also a dialysis technique can be used, in which the common solvent is gradually replaced with a selective solvent. (ii) The second technique is directly dissolving the polymer in the selective solvent, and is then let to anneal e.g. by thermal treatment.

Determination of the CMC for different block copolymer systems, has been done with a number of methods, e.g. static light scattering, surface tension measurements, steady state fluorescence and fluorescence correlation spectroscopy. In table 1.1 the measured CMC for some chemically different block

Table 1.1 CMC values, at 25°C, for some chemically different block copolymers in aqueous solution. The subscript gives the number of monomers in a block.

Polymer	Ref.	CMC [M]	Method[(a)]
P[(Ethylene oxide)$_{102}$-*b*-(Propylene oxide)$_{37}$]	[40]	9.5×10^{-3}[(b)]	ST
P[(Ethylene oxide)$_{102}$-*b*-(Propylene oxide)$_{37}$]	[41]	4.1×10^{-3}[(b)]	SLS
P[(Ethylene oxide)$_{18}$-*b*-(Butylene oxide)$_{9}$]	[42]	2.1×10^{-5}	ST
P[(Styrene)$_{23}$-*b*-(*tert*-butyl acrylate)$_{300}$]	[43]	5×10^{-6}	SSF
P[(Ethylene glycol)$_{122}$-*b*-(D-lactide)$_{29}$]	[44]	5×10^{-7}	SSF
P[(Isobutylene)$_{70}$-*b*-(Methacrylic acid)$_{52}$]	[45]	3.6×10^{-8}	FCS

(a) ST: Surface Tension, SLS: Static Light Scattering, SSF: Steady State Fluorescence, FCS: Fluorescence Correlation Spectroscopy. (b) Measured at 20°C.

copolymers determined with different methods is shown. When the CMC is relative high ($\gtrsim 10^{-5}$ M, depending on the polymer) the CMC can be determined with static light scattering or surface tension measurements. If the CMC is at a lower lower concentration, which is often the case with diblock copolymers [1], other methods must be applied. Therefore determinations are made using a tracer whose properties change with the formation of micelles. One such method is steady state fluorescence where the fluorescence properties of e.g. pyrene are measured. Pyrene has a low solubility in aqueous solution and therefore it is expected that when micelles are formed, pyrene will preferentially be present in the micellar core, whereby the fluorescence properties of pyrene will change [46]. Another method where tracers are used to determine the CMC, is fluorescence correlation spectroscopy, where the diffusion coefficient of the tracer is determined. If the tracer is hydrophobic and will preferential be present in micelles, the CMC can be determined as a change in the diffusion coefficient [45, 47, 48]. The problem with tracer experiments is, that the tracer can influence the aggregation behavior and differences between micellar hydrodynamic radius in tracer experiments and photon correlation spectroscopy have been observed [45, 48, 49].

1.1 Poly(2-alkyl-2-oxazoline)

The polymer system we have investigated is based on poly(2-alkyl-2oxazoline), which constitutes a versatile system to investigate the aggrega-

tion behavior. In contrast to other systems, e.g. the well studied Pluronics system, the degree of hydrophobicity can be varied, and additional functional groups can be introduced in the polymer side chains as well as the chain termini. Figure 1.4 shows the 2-substituted-2-oxazoline monomer. The poly-

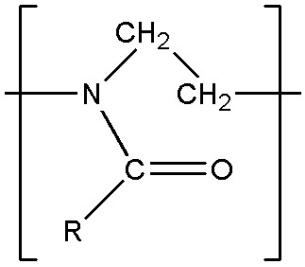

Figure 1.4 Monomer of 2-substituted-2-oxazoline. The group R can be substituted with e.g. an alkyl-chain or functionalized groups.

mers in this study are based on 2-alkyl-2-oxazoline, where the hydrophobicity can be changed by varying the length of the alkyl side-chain. 2-methyl- and 2-ethyl-2-oxazoline are hydrophilic, whereas longer side groups will result in increasing hydrophobicity [50]. With these types of polymers, a great variety of polymer architecture is possible, such as homopolymers, diblock and triblock copolymers, random copolymers, stars, dendrimers and lipopolymers [51, 52, 53]. Poly(2-oxazoline) has been found to be biocompatible and non-toxic [54] and is thus under intense study for biological and biomedical applications, such as drug delivery systems [55] and for the construction of artificial cell membranes [56, 57]. The possibility to functionalize the polymer side chains and termini, has led to the synthesis of novel amphiphilic block copolymers for micellar catalysis [58]. Furthermore, there is the possibility to attach a fluorescence dye to the polymer.

1.2 The present study

The main part of this rapport concerns the aggregation behavior of poly(2-alkyl-2-oxazoline) based block copolymers. Poly(2-methyl-2-oxazoline) has been used as the hydrophilic part and poly(2-nonyl-2-oxazoline) as the hydrophobic part. These types of copolymers are expected to have a low CMC, because of the high hydrophobicity that the nonyl side-chains causes. We therefore expected that the CMC was so low, that it would be impossible or very difficult to measure with standard methods (light scattering, surface

tension). The aggregation behavior was therefore measured using fluorescence correlation spectroscopy, which can measure at very low concentration (down to nM). Fluorescence labeled polymers are used as fluorescence tracers in the experiment. In the literature, FCS has been used to determine very low CMC's, using tracers that were not identical to the polymers [45, 46, 47, 48]. We use a polymeric tracer, where the polymers have been labeled with a fluorescence dye. Solutions of labeled and non-labeled but otherwise identical polymers were used. In this manner, we are able to cover a large concentration range. From the concentration dependence of the diffusion coefficient, determined with FCS, we are thus able to determine the CMC. The diffusion coefficient was also measured using photon correlation spectroscopy, to investigate the influence of the polymeric tracer on the diffusion coefficient. Also the size of the diblock copolymer aggregates was measured using small angle neutron scattering.

In total, the diffusion coefficients of four different polymer architectures were measured using FCS: Homopolymers, diblock copolymers, triblock copolymers (ABA-type) and random copolymers.

2 Experimental

2.1 Polymer samples

The polymer samples under investigation are all based on poly(2-alkyl-2-oxazoline). In this type of systems, the hydrophobicity of the polymers can be varied, by changing the alkyl side group: 2-methyl- and 2-ethyl-2-oxazoline are hydrophilic, whereas side groups longer than propyl result in increasing hydrophobicity [50].

Four different polymer architectures have been investigated, namely homopolymers, diblock copolymers, triblock copolymers and a random copolymer. For the homopolymers as well as the hydrophilic part of the block copolymers, poly(2-methyl-2-oxazoline) (P(MOx)) have been used and as hydrophobic part for the copolymers poly(2-*n*-nonyl-2-oxazoline) (P(NOx)) have been used. The idea was, that for the different block copolymers, the degree of polymerization of P(NOx) was kept constant. The polymers investigated are collected in table 2.1. The polymers investigated by FCS were first synthesized and terminated with piperazine. A small fraction of the polymers were then fluorescence labeled, so that identical polymers with and without the fluorescence label were obtained. In the table, the molar mass given is the one of the non-labeled polymer. By synthesizing both labeled and non-labeled polymer a large concentration range in the FCS measurements could be covered.

One polymer ($P(MOx)_{22}$) was labeled with aminofluorescein (AF). AF has the disadvantage, that the FCS measurements have to be done in a buffer with pH 9, because AF has a pH-sensitive fluorescence emission which is significantly reduced below pH 7.0. Furthermore, AF is known to have a high rate of photobleaching [59].

The fluorescence label used for all other polymers, is tetramethyl rhodamine isothiocyanate (TRITC). It was chosen because it had suitable fluorescence properties (absorption at 544 nm and emission at 572 nm), a good photostability, and there is no need to use a buffer, meaning that pure water can be

Table 2.1 Characteristics of the investigated polymers.

Polymer	w_{NOX}	$\overline{M}_n$ [g mole^{-1}]	$\overline{M}_w/\overline{M}_n$
Homopolymers			
$P(MOx)_{13}$	0	1,205	1.19
$P(MOx)_{22}$ [(a)]	0	1,970	1.18
$P(MOx)_{26}$	0	2,310	1.21
$P(MOx)_{45}$	0	3,930	1.10
$P(MOx)_{60}$	0	5,220	1.58
Diblock copolymers			
$P[(MOx)_{40}(NOx)_7]$	0.15	4,034	1.20
$P[(NOx)_{10}(MOx)_{32}]$	0.23	4,796	1.07
$P[(NOx)_6(MOx)_{30}]$ [(b)]	0.17	4,046	1.10
Triblock copolymers			
$P[(MOx)_{20}(NOx)_7(MOx)_{14}]$	0.17	4,380	1.40
$P[(MOx)_{30}(NOx)_7(MOx)_{26}]$	0.11	6,250	1.35
Random copolymer			
$P[(MOx)_{40}(NOx)_6]_{\mathrm{random}}$	0.13	4,690	1.38

(a) Labeled with AF
(b) This sample was used for small angle neutron scattering.
w_{NOX} is the number fraction of P(NOx) of the polymer, $\overline{M}_n$ is the molar mass of the non-labeled polymer determined by ^{1}H-NMR and $\overline{M}_w/\overline{M}_n$ is the polydispersity ($\overline{M}_w$ and $\overline{M}_n$ are the weight average and number average molar mass, respectively) determined with gel permeation chromatography.

used as solvent, instead of a buffer [59].

All polymers were synthesized, fluorescence labeled and characterized by ^{1}H NMR and gel permeation chromatography by Karin Lüdtke and Thomas Komenda at the Chemistry Department, TU München.

2.1.1 Homopolymers

The homopolymers under study are all based on P(MOx), which is water soluble [50]. AF and TRITC were used as fluorescence labels. Figure 2.1A shows the structure of $P(MOx)_{22}$ labeled with AF. This is the only polymer labeled with aminofluorescein because, as already mentioned, the fluorescence

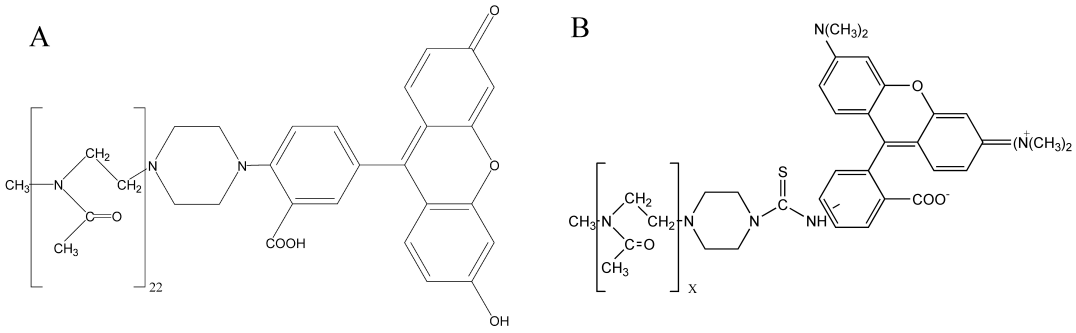

Figure 2.1 The structure of $P(MOx)_{22}$ labeled with aminofluorescein (A) and the structure of $P(MOx)_x$ labeled with TRITC, where x is the degree of polymerization (B).

properties are very dependent on pH.

The other four homopolymers were labeled with the fluorescence dye TRITC. This structure is shown in figure 2.1B. The fluorescence dye used is a mixture of two isomers (tetramethyl rhodamine-5-isothiocyanate and tetramethyl rhodamine-6-isothiocyanate). The molar mass of the dye is 433.52 g $mole^{-1}$, which means, that it is not negligible compared to the molar mass of the homopolymers (which is in the range 1200 and 5200 g $mole^{-1}$).

2.1.2 Diblock copolymers

Two different diblock copolymers have been studied. The fluorescence label, TRITC, is either attached to the end of the hydrophilic or to the end of the hydrophobic block, see figure 2.2. The reason that two polymers, with different position of the fluorescence label were used, was to investigate the influence of the position of the dye. As seen from the 3D structure in figure 2.3, the volume of the label is small compared to the one of the diblock copolymer.

2.1.3 Triblock copolymers

The investigated triblock copolymers are of the ABA-type, where A and B denote the hydrophilic (P(MOx)) and hydrophobic block (P(NOx)), respectively. Both triblock copolymers were obtained in fluorescence labeled and non-labeled form. The fluorescence label is for both polymers, attached at

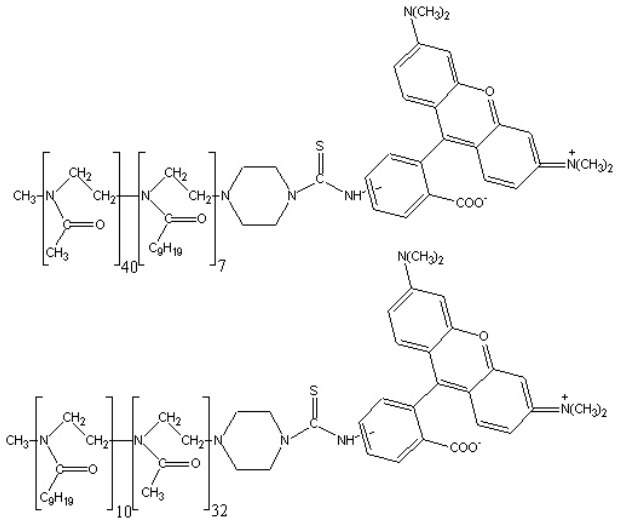

Figure 2.2 Structure of the two diblock copolymers. The polymer on top and bottom has the fluorescence label attached to the hydrophobic part and hydrophilic part, respectively.

the end of one of the hydrophilic blocks. The overall degree of polymerization for one of the triblock copolymers was meant to resemble the ones of the diblock copolymers, whereas the other triblock copolymer has a larger hydrophilic content. The degree of polymerization of the hydrophobic blocks are equal for both triblock copolymers, but the degree of polymerization of the hydrophilic block is varied.

2.1.4 Random copolymer

One random copolymer was studied, consisting of MOx and NOx groups (figure 2.4). Unlike the block copolymers, the random copolymer has the monomers randomly distributed. The overall degree of polymerization was again chosen to resemble the overall degree of polymerization of the diblock copolymers.

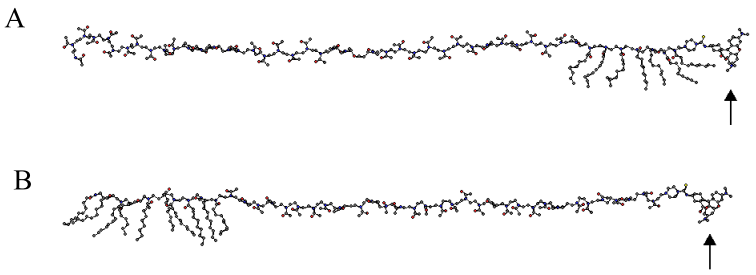

Figure 2.3 3D structures of the two diblock copolymers: (A) P[$(MOx)_{40}(NOx)_7$] and (B) P[$(NOx)_{10}(MOx)_{32}$], which has the fluorescence label, TRITC attached at the end of the hydrophobic and hydrophilic block, respectively. The fluorescence label is indicated by the arrows. The 3D structures has been generated with CS Chem 3d ultra 7.0.0. [60]. The overall stretched configuration is not necessary the equilibrium structure.

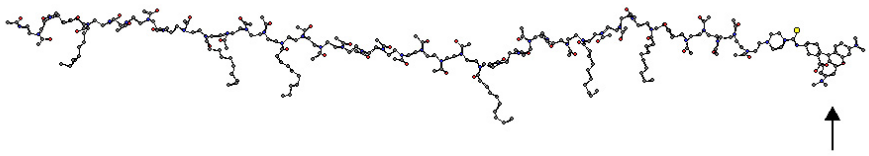

Figure 2.4 One possible 3D structure of the random copolymer, P[$(MOx)_{40}$-$(NOx)_6$]$_{random}$. The hydrophobic part (2-*n*-nonyl-2-oxazoline) can be recognized by the long side chains (as compared to 2-methyl-2-oxazoline). The fluorescence dye, TRITC, is indicated by the arrow.

2.2 Fluorescence correlation spectroscopy

The idea of fluorescence correlation spectroscopy (FCS) was originally introduced by Magde, Elson and Webb in a series of papers, where they presented the theory and the first experimental setup [61, 62, 63]. FCS is a method to determine diffusion coefficients by measuring the time-dependent fluorescence signal and correlate it. Because it is the fluctuations of the fluorescence signal that is measured, is is an advantage when the measurements are based on a few molecules, since the relative fluctuations are higher. In the first FCS experiments, the average number of fluorescence molecules in the detection volume was around 10,000 [61, 63] and was still able to extract the motion of individual molecules [64]. Even though FCS showed great potential from the beginning, it did not become widespread until recently. There were problems with a high background (due to large detection volumes), low detection yields meant that long measurement times were needed and high concentrations of the fluorescence species were needed to compensate for the high background. With the introduction of extremely small detection volumes, confocal optics, highly sensitive avalanche photodiode detectors and selective bandpass filters to discriminate fluorescence from the background, the signal-to-background ratio could be improved by several orders of magnitude [65, 66]. With these improvements to the FCS setup, the average number of molecules in the detection volume can be kept low without compromising the signal level, and the measurement times could be shortened drastically.

2.2.1 The principle of FCS

As already mentioned, FCS is a method based on measuring the intensity fluctuations, arising from fluorescence bursts in a very small detection volume. The fluorescence bursts are detected by a single photon detector, and the signal is autocorrelated.

The principle of the FCS setup is shown in figure 2.5. Laser light is guided to the instrument and is reflected by a dichroic mirror. The beam is then focussed into the sample by a water immersion microscope lens. The emitted fluorescent light is collected through the same optics as the excitation laser, but passes through the the dichroic mirror and furthermore through an emission filter, which discriminates i.e. the excitation wavelength. In order to only collect the emitted fluorescence light from a defined volume in the sample, confocal optics are used (shown as a lens and pinhole in figure 2.5) to ensure that emitted fluorescence outside the detection volume are not

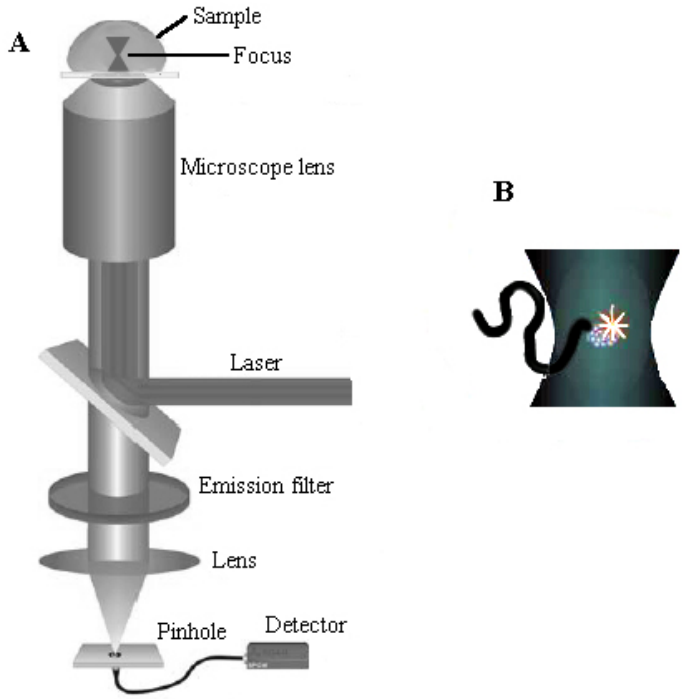

Figure 2.5 The principle of the fluorescence correlation spectrometer. (A) shows the principle of the setup, where laser light is focussed into the sample by a microscope lens. When fluorescence molecules are in the focus, they are excited and emits fluorescent light, which is collected by an avalanche photodiode. (B) shows the focus, where fluorescence molecules emits fluorescent light. Both drawings are taken from [67].

collected. The resulting detection volume in the sample is in the order of 1 μm^3 (10^{-15} liter). The time-dependent fluorescence signal is detected by a single-photon counting avalanche photodiode. The autocorrelation function is calculated in real-time from the time-resolved fluorescence intensity by a correlator.

2.2.2 Experimental

All FCS measurements shown here, are made using a ConfoCor2 from *Carl Zeiss Jena* GmbH, equipped with a C-Apochromat $40\times/1.2$ water immersion microscope lens and a motorized pinhole with a diameter of 80 μm. Lab-tek 8-well chambered coverglass from Nalge Nunc International was used as sample chamber for all FCS measurements. The measurement-time is between 10

and 30 seconds. The measurements are repeated 10 times and the correlation functions are averaged. This procedure was repeated at minimum 3 times. The measurements were done in a climatized room, since there no temperature control was available. The measurements were done in a temperature range of 20-25°C . The calibration of the focus was done using rhodamine 6G (Sigma-Aldrich) and the determined structure factor was always in the range $S = 5 - 6$. Two different excitation wavelengths were used, depending on the fluorescence dye.

When the AF-labeled polymer was used as a tracer, an Argon-ion laser operated at 488 nm was used. A band pass filter, which is only transparent for wavelengths in the range 530 - 600 nm, was used as an emission filter. The laser power was attenuated to 0.1 - 1.0% of the maximum power of $\simeq 1.8$ mW [68], in order to avoid bleaching of the dye molecules. The count rate was typically between 10 and 100 kcts/s, depending on the attenuation. As the fluorescence emission of aminofluorescein is significantly lowered below pH = 7.0, a sodium tetraborate ($Na_2B_4O_7 \cdot 10\ H_2O$)/ hydrochloric acid (HCl) buffer solution (pH = 9.0, Fluka Chemika) was used as a solvent.

When the TRITC labeled polymers were used as a tracer, a HeNe laser at 543 nm and a band pass filter transparent for wavelengths in the interval 560 - 615 nm, was used. The laser power was attenuated to 1 - 3 % of the maximum power of $\simeq 0.23$ mW [68]. The count rate was typically in the range 10-30 kcts/s. Stock solutions of the polymers were prepared in deionized and filtered water at room temperature.

The homopolymers were prepared at room temperature. The diblock copolymers were first measured as prepared at room temperature. The measurements of the diblock copolymers were repeated, after the stock solution had been measured by temperature-resolved PCS (see section 2.3.1), i.e. the samples had been heated to at least 90°C . Stock solutions of non-labeled triblock copolymers and random copolymers were heated to 80°C for at least 12 hours. The stock solutions of the corresponding labeled and non-labeled polymers were mixed with water in appropriate ratios shortly before measurement.

The fluorescence background of the solvent and solutions of non-labeled polymers was measured, and it was negligible compared to the fluorescence signal from solutions of labeled polymers.

2.2.3 Data analysis

Fluorescence light in the detection volume is detected and correlated. If it is assumed that the excitation power is constant, the fluctuations of the

fluorescence signal are defined as the difference between the average and the time-dependent fluorescence signal, $F(t)$:

$$\delta F(t) = F(t) - \langle F(t) \rangle \tag{2.1}$$

where $\langle F(t) \rangle$ is the time-averaged fluorescence signal. The normalized auto-correlation function reads

$$G(\tau) = \frac{\langle \delta F(t)\, \delta F(t+\tau) \rangle}{\langle F(t) \rangle^2} \tag{2.2}$$

If only concentration fluctuations of the fluorescence molecules are considered (i.e. no change in the fluorescence properties dye to chemical reactions) and the detected volume is assumed to be a three dimensional Gaussian (which is decayed to $\frac{1}{e^2}$ at z_0 and w_0), the following expression can be derived [62, 69]

$$G(\tau) = \frac{1}{V_{eff}\langle C \rangle} \left(\frac{1}{1+\frac{\tau}{\tau_D}} \sqrt{\frac{1}{1+\frac{\tau}{S^2\tau_D}}} \right) \tag{2.3}$$

where V_{eff} is the effective detection volume, $\langle C \rangle$ is the average concentration of fluorescence molecules, τ is the lag-time, τ_D is the diffusion time through the detection volume and S is the axial ratio of the detection volume, $S = {}^{z_0}/_{w_0}$ (also known as the "structure factor"), where z_0 and w_0 are the half-hight and half-width of the detection volume, respectively. From the determined diffusion time the diffusion coefficient and hydrodynamic radius can be determined by [62]

$$\tau_D = \frac{w_0}{4D} \tag{2.4}$$

where D is the diffusion coefficient.

Figure 2.6 shows 7 different correlation functions with different diffusion time. Since diffusion time and diffusion coefficient are inversely proportional (see equation 2.4) and thus the hydrodynamic radius is proportional to the diffusion time (see equation 2.10) this curve shows the effect of particle size on the FCS correlation curves, with increasing particle size, the diffusion time increases, e.g. the diffusion coefficient decreases.

In equation 2.3, the first factor, ${}^{1}/_{V_{eff}\langle C \rangle}$, corresponds to the inverse of the average number of particles in the detection volume. Figure 2.6B shows the effect of concentration on the correlation function, for particles of the same size. It can be seen, that if the number of particles in the detection volume is increased (e.g. the concentration of fluorescence particles is increased), the

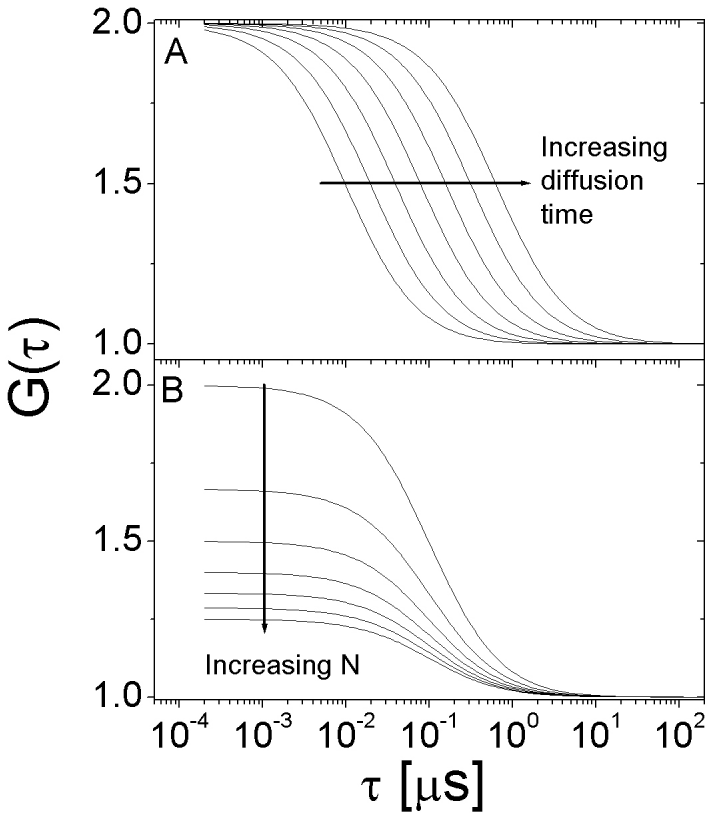

Figure 2.6 A: Autocorrelation functions for different diffusion times. The diffusion times are in the range 0.01 - 0.64 μs with a factor of two between two neighboring curves. B: Autocorrelation functions with constant diffusion time (τ_D = 0.1 μs), but with different number of particles in the detection volume, N. N is in the range of 1 - 4 and is varied in steps of 0.5. In all curves the structure factor has been set to $S = 6$.

amplitude of the correlation function decreases. In order to get highest possible resolution of the correlation function, the number of fluorescence particles in the detection volume (i.e. the concentration of fluorescence molecules) has to be as low as possible.

Triplet decay

So far, it has been assumed that the fluorescence properties are not changing while the particle is in the detection volume. This assumption does not hold for real situations. The most common problem is the transition of the dye

to the first excited triplet state. During this time, the dye cannot emit any fluorescence burst and appears dark. Instead of recalculating the correct autocorrelation function for these slightly altered conditions, a much simpler and general form is used. If intra- or intermolecular reactions give rise to fluorescence fluctuations on time scales much faster than those caused by the motion of particles, a separation of the dynamics is possible [67]:

$$G(\tau) = G_{\text{motion}}(\tau) \cdot X_{\text{kinetics}}(\tau) \tag{2.5}$$

This assumption holds only for situations, in which the diffusion coefficient is unaltered by the reaction, which is the case with triplet blinking [70]. The triplet blinking described above can be described by a simple exponential decay [71]:

$$X_{\text{triplet}} = 1 + \frac{F}{1-F} \exp\left(-\frac{\tau}{\tau_T}\right) \tag{2.6}$$

where F is the triplet fraction and τ_T is the triplet time.

If equations 2.3, 2.5 and 2.6 are combined, the overall autocorrelation function for a freely diffusing fluorescentce molecule can be written as

$$G(\tau) = 1 + \frac{1}{N}\left(\frac{1}{\left(1+\frac{\tau}{\tau_D}\right)\sqrt{1+\frac{\tau}{S^2\tau_D}}}\right)\left[1 + \frac{F}{1-F}\exp\left(-\frac{\tau}{\tau_T}\right)\right] \tag{2.7}$$

This is an expression for the normalized correlation function in FCS, for the case of one type of diffusing fluorescence molecules being present in the detection volume.

Measurement of one fluorescence species

Figure 2.7 shows an example of a correlation function for Rhodamine 6G (Rh6G), which is a standard fluorescence dye that is used for determination of the width of the detection volume and the structure parameter. This is accomplished by performing a measurement of a low concentration of this dye (in the range of 1×10^{-8} M) and from the fit of the correlation function, the diffusion time and the structure factor can be determined. Since the diffusion coefficient of Rh6G is known, $D = 2.8\times10^{-10}$ m^{2}s^{-1} [63], the width can be determined by equation 2.4.

The line in figure 2.7 is a it of equation 2.7, and the the diffusion time, as well as the structure factor are found. From the diffusion time, w_0 can be

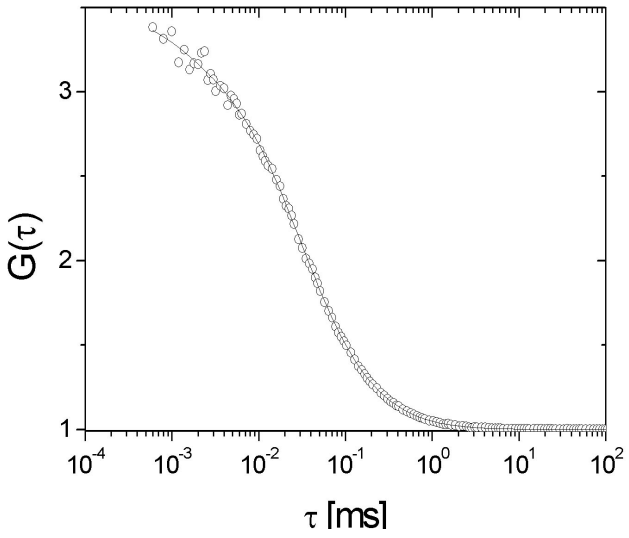

Figure 2.7 The correlation function of Rhodamine 6G (○). The line is a fit of equation 2.7. The parameters extracted from the fit are $\tau_D = 30 \pm 0.6$ μs, $\tau_T = 1.3 \pm 0.3$ μs, $F = 0.09 \pm 0.01$ and $N = 0.44 \pm 0.01$.

calculated by

$$w_0 = \sqrt{4D_{Rh6G}\tau_{D,Rh6G}} \tag{2.8}$$

When the diffusion time of a sample, $\tau_{D,s}$, is found, the diffusion coefficient, D_s, can be calculated by

$$D_s = \frac{D_{Rh6G}\ \tau_{D,Rh6G}}{\tau_{D,s}} \tag{2.9}$$

All polymer diffusion coefficients have been calculated in this way. From the diffusion coefficient, the hydrodynamic radius, r_H, can be calculated using the Stokes-Einstein equation [72]

$$r_H = \frac{k_B T}{6\pi\eta D} \tag{2.10}$$

where k_B is Boltzmann's constant, T is the absolute temperature and η is the solvent viscosity.

Multiple fluorescence species

Until now, it has been assumed that only one type of fluorescence molecules is present in the detection volume. If two or more different types of fluorescence molecules, with different diffusion coefficients, are present in the detection volume, the correlation function is the sum of the correlation function of each species:

$$G(\tau) = \left(1 + \frac{F}{1-F}\exp\left(-\frac{\tau}{\tau_T}\right)\right)\left(\frac{1}{N}\sum_{i=1}^{k}\rho_i g_i\right) + 1 \tag{2.11}$$

where g_i is given by

$$g_i = \frac{1}{\left(1+\frac{\tau}{\tau_{D,i}}\right)\sqrt{1+\frac{\tau}{S^2\tau_{D,i}}}} \tag{2.12}$$

and ρ_i is the relative amplitude corresponding to molecules with identical diffusion coefficient, which are related to the concentration, c_i, by:

$$\rho_i = \frac{\phi_i^2 c_i}{\sum_{i=1}\phi_i^2 c_i} \tag{2.13}$$

where ϕ_i is the quantum yield of the i-th species. If the quantum yield is the same for all diffusing species, the amplitude is equal the molecular fraction. Figure 2.8 shows the calculated correlation functions for two fluorescence species, with different diffusion times. The diffusion times has been held constant, but the fraction of the two species has been varied.

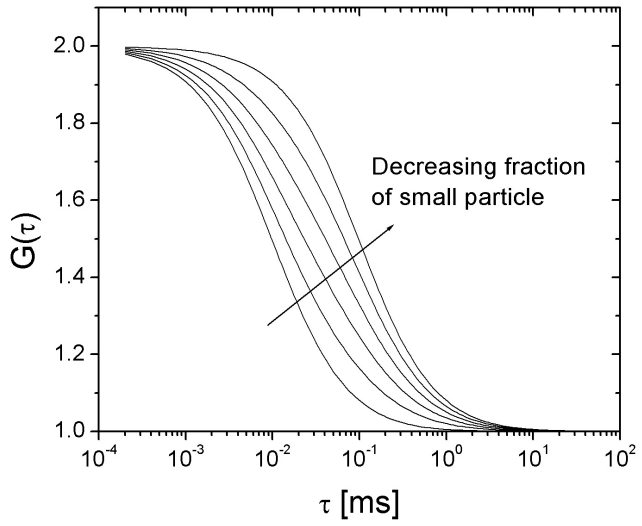

Figure 2.8 Correlation functions of two species, where the number fraction (amplitude) has been varied. The particle sizes are kept constant (τ_D is 0.01 and 0.1 ms for the small and large specie, respectively), but the amplitude have been varied. The amplitude of the small particle is (from left to right) 1, 0.8, 0.6, 0.4, 0.2 and 0.

2.3 Photon correlation spectroscopy

Photon correlation spectroscopy (PCS) is a widely used technique to determine, among others, diffusion coefficients in dilute solution [73, 74]. In FCS the number fluctuations of the fluorescence dye was measured, whereas in PCS the distance fluctuations of the particles. For distance fluctuations, it is necessary that the measurements are based on many particles. Therefore is the measurement volume in PCS is larger ($\sim$mm^3) compared to FCS.

The principle of the PCS setup used is shown in figure 2.9. The sample is

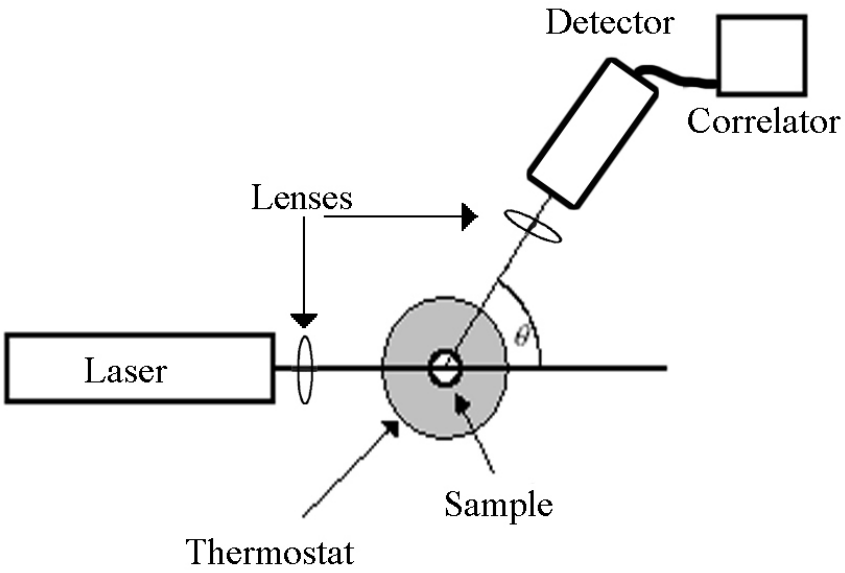

Figure 2.9 The principle of PCS. The laser light is scattered by the sample, which is placed in a thermostat, and the time-dependent intensity signal is measured at the angle θ and autocorrelated.

placed in a thermostat in order to control the temperature. The laser is focussed into the sample, and the scattered light is detected at the scattering angle, θ. For detection, two APD detectors are used, working in pseudo

cross-correlation, to avoid artifacts in the early time regime of the correlation function.

2.3.1 Experimental

The PCS measurements were performed in the laboratory of Dr. Petr Štěpánek, Institute of Macromolecular Chemistry, Academy of Sciences of the Czech Republic, Prague, in the Czech Republic.

Temperature-resolved PCS measurements were performed using an ALV-5000/E logarithmic correlator together with a goniometer with an index-matching vat filled with decalin, to match the refractive index of the glass scattering cell. The light source was a HeNe laser operated at 633 nm. The scattered light was collected at a fixed scattering angle of 90°.

The correlation functions of two non-labeled diblock copolymers, P[$(MOx)_{40}$-$(NOx)_7$] and P[$(NOx)_{10}(MOx)_{32}$] were measured with temperature-resolved PCS at different concentrations. The polymers were dissolved in distilled water and, in order to avoid dust in the samples, they were filtered into previously de-dusted scattering cells and were sealed at room temperature. The measurement time was 30 minutes, and there was 30 minutes waiting time between each measurement, in order to ensure thermal equilibrium.

2.3.2 Data analysis

The PCS correlation function is given by [13]

$$G_2(\tau) \equiv \lim_{T_E \to \infty} \frac{1}{T_E} \int_0^{T_E} I\,(t)\, I\,(t+\tau)\, dt \tag{2.14}$$

where $I\,(t)$ is the intensity of the scattered light at time t, $I\,(t+\tau)$ is the intensity of scattered scattered light after a delay time τ and T_E is the overall experimental time. The normalized correlation function is defined as

$$g_2\,(\tau) = \frac{G_2\,(\tau)}{G\,(\infty)} \tag{2.15}$$

where $G\,(\infty)$ is the correlation at $\tau = \infty$ (baseline). In case of several decays in the correlation function, $g_2\,(\tau)$ can be written as [75]

$$g_2(\tau) - 1 = \gamma \left[\int_0^{\infty} \tau_r A(\tau_r) \exp\left(-{}^{\tau}/_{\tau_r}\right) d\left(\ln\left(\tau_r\right)\right) \right]^2 \tag{2.16}$$

where γ is an instrumental constant and $A(\tau_r)$ is the distribution of relaxation times. To analyze the PCS correlation function, the fitting routine REPES [76] has been applied. REPES is a part of the program GENDIST [77] which was used to analyze the data. The program calculates the distribution $A(\tau_r)$ by an inverse Laplace transformation of g_2. From the centers of gravity of the peaks of $A(\tau_r)$, the diffusion coefficient is obtained by using [78]

$$D = \frac{\Gamma}{q^2} \tag{2.17}$$

where Γ is the relaxation rate ($\Gamma = \tau_r^{-1}$) and q is the length of the scattering vector given by

$$|\vec{q}| = q = \frac{4\pi n}{\lambda} \sin\left(\frac{\theta}{2}\right) \tag{2.18}$$

where n is the refractive index of the solvent, λ is the wavelength and θ is the scattering angle. The hydrodynamic radius is calculated using the Stokes-Einstein equation (equation 2.10). The temperature dependent viscosity of water is included in the GENDIST program used for analysis.

2.4 Small-angle neutron scattering

Small-angle neutron scattering (SANS) was used to verify and characterize the non-equilibrium aggregates, observed with PCS. SANS is a method to determine the structure and size of particles by measuring the intensity of scattered neutron in dependence of the scattering angle, θ [79].

The principle of the SANS setup can be seen in figure 2.10. The neutrons

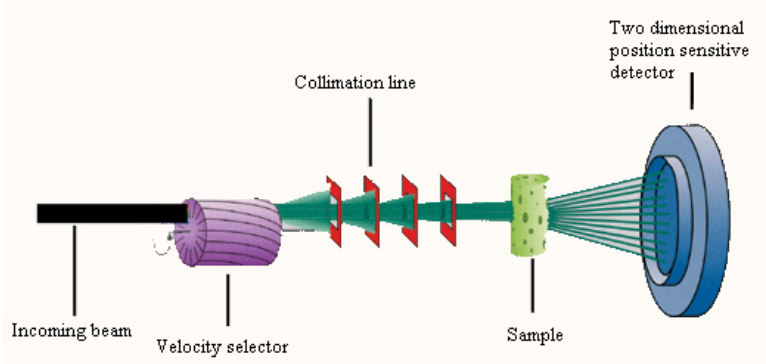

Figure 2.10 The principle of small-angle neutron scattering. The neutron comes from the source and is scattered by the sample. The scattered intensity at different scattering angles, θ, is measured by a two-dimensional detector. From [80].

are guided from the neutron source to the velocity selector. The initial distribution of wavelengths is very broad, and the velocity selector results in a narrower distribution of neutron wavelengths. The beam is collimated in order to get a parallel beam. The collimated neutron beam is then scattered by the sample. The scattered neutrons are detected by a two-dimensional position-sensitive detector.

2.4.1 Experimental

SANS measurements were performed at the SANS-2 instrument at the GKSS-Forschungszentrum Geesthacht. The neutron wavelength was 5.8 Å. The detector distances used for the experiments were 1, 3, 9 and 21 meters, which corresponds to q-ranges of 0.44 - 2.6 nm^{-1}, 0.13 - 0.87 nm^{-1}, 0.43 - 0.29 nm^{-1} and 0.016 - 0.12 nm^{-1}, respectively. The measuring times were 30, 60, 90 and 120 minutes for the detector distances of 1, 3, 9 and 21 meters, respectively. The background was determined with a sample of D_2O and was subtracted from the scattering curves.

The differential cross section was calculated by [81]

$$\frac{d\sigma(\vec{q})}{d\Omega} K_g = I(\vec{q}) \tag{2.19}$$

where K_g is a constant given by the geometrical configuration, the intensity of the incident flux and the sample transmission. The transmission of the samples was measured at every position and the incident flux was calibrated using a vanadium standard. The program SANDRA ver. 4.2.1 [82] was used to construct the curves from the different measured distances and to calculate the differential cross section.

Table 2.2 Calculated scattering length densities.

	ρ [$\times 10^{10}$ cm^{-2}]
P(MOx)	1.3
P(NOx)	2.7
H_2O	-0.56
D_2O	6.4

The scattering lengths of P(MOx), P(NOx), H_2O and D_2O, calculated by equation 2.23 are shown in table 2.2. The values have been calculated on the basis of values for the scattering lengths of the elements found in ref. [81] and densities of 1.14 g cm^{-3} for P(MOx) [83][1] and 1.01 g cm^{-3} for P(NOx) [50]. To get the largest contrast for the entire micelle, the measurements were performed en D_2O, which has the largest contrast for the two blocks of the block copolymer. The polymer solution was prepared at room temperature at a polymer concentration of 0.014 M and was put in a quartz cuvette. After the measurement, the sample was annealed at 60°C for 24 hours and was then measured once more.

2.4.2 Data analysis

The amplitude of neutron radiation scattered from scattering objects located at $\vec{r_i}$, each characterized by a scattering length b_i is given by [84]

$$f(q) = \sum b_i \exp\left(i\vec{q} \cdot \vec{r_i}\right) \tag{2.20}$$

[1]This value is for 2-ethylene-2-oxazoline, but the density of 2-methyl-2-oxazoline is expected to be similar.

where $\vec{q}$ is the scattering vector (see equation 2.18). The intensity, $I(\vec{q})$, is proportional to the square of the scattering amplitude

$$I(\vec{q}) = K_g \left| f(\vec{q}) \right|^2 \tag{2.21}$$

where K_g is given by the geometrical configuration, the intensity of the incident beam and the sample transmission. Normalization with respect to these parameters gives the differential cross-section, $^{d\sigma(\vec{q})}/_{d\Omega}$

$$\frac{d\sigma(\vec{q})}{d\Omega} = \sum \sum b_i b_j \exp\left(i\vec{q} \cdot \vec{r}_{ij}\right) \tag{2.22}$$

where σ is the number of detected particles per time unit and incident flux, and Ω angular volume. In small-angle scattering the resolution is not on atomic distances and the discrete scattering lengths can therefore be replaced by a continues function, called the scattering length density [81]

$$\rho_s = \sum_i \frac{b_i}{V_m} \tag{2.23}$$

where V_m is the molecular volume. Defining the scattering length density correlation function

$$\tilde{\gamma}_{ij} \equiv \tilde{\gamma}\left(\vec{r}_{ij}\right) \equiv \rho\left(\vec{r}_i\right) \rho\left(\vec{r}_j\right) \tag{2.24}$$

gives the general expression of the differential cross section [84]

$$\frac{d\sigma(\vec{q})}{d\Omega} = \int_{\text{sample}} \tilde{\gamma}\left(\vec{r}\right) \exp\left(i\vec{q} \cdot \vec{r}\right) d\vec{r} \tag{2.25}$$

The scattering length density can be replaced by the function η_s, which describes the fluctuations from the average

$$\eta_s\left(\vec{r}\right) = \rho\left(\vec{r}\right) - \langle \rho \rangle \tag{2.26}$$

With the normalized correlation function

$$\gamma_{ij} = \frac{\eta_{s,i}\eta_{s,j}}{\langle \eta_s^2 \rangle} \tag{2.27}$$

the scattering function can be written as [84]

$$\frac{d\sigma(\vec{q})}{d\Omega} = \langle \eta_s^2 \rangle \int_{\text{sample}} \gamma\left(\vec{r}\right) \exp\left(i\vec{q} \cdot \vec{r}\right) d\vec{r} \tag{2.28}$$

For a dilute solution of identical, randomly oriented particles, the scattering function reads [84, 85]

$$\frac{d\sigma(q)}{d\Omega} = \langle \eta_s \rangle 4\pi N_\nu \int r^2 \gamma(r) \frac{\sin(qr)}{qr} dr \tag{2.29}$$

where N_ν is the number of particles per volume. The term $r^2\gamma(r)$ is the so-called pair distance-distribution function, $p(r)$, that can be determined by Fourier transformation of the measured cross-section. However, the experimental data are measured only over a limited q-range and also noise in the measured data, gives problems with the Fourier transform. Therefore an alternative method has been used to determine $p(r)$, namely the indirect Fourier transform [85, 86], where $p(r)$ is expressed as a linear combination of M cubic b-spline functions, $B_i(r)$

$$p(r) = \sum_{i=1}^{M} d_i B_i(r) \tag{2.30}$$

where d_i are coefficients of the cubic b-spline functions. The Fourier transform of $p(r)$ is the scattered intensity, $I(q)$, which then can be written as

$$I(q) = \sum_{i=1}^{M} d_i C_i(q) \tag{2.31}$$

where C_i is the Fourier transform of B_i. The coefficients, d_i, are determined by a least square fit of equation 2.31 to the measured $I(q)$.

The SANS data has been analyzed using the computer program GIFT (Generalized Indirect Fourier Transformation). The version of GIFT used, is a part of PCG software version. 1.01.02, developed at the university of Graz [87]. In the software, there is additionally the opportunity to take into account, that the particles interact with each other [88]. The particles have been treated as hard spheres when analyzing the SANS data.

3 Results and Discussion

In this chapter, the results from the performed measurements are shown and discussed.

In section 3.1 the measured diffusion coefficient for the homopolymers are shown. The diffusion coefficients were determined as function of concentration and degree of polymerization. Modelling of both functionalities have been attempted.

In section 3.2 the results for the diblock copolymers are shown. The concentration dependence of the diffusion coefficient for the diblock copolymers were measured with FCS and PCS. In this manner the CMC could be determined. The concentration dependent amplitude of the micelles, as found with FCS, was modelled using the closed association model. Also SANS was performed on one polymer concentration.

In section 3.3 the FCS measurements of the triblock copolymers and the random copolymer is shown. The concentration dependence of the diffusion coefficients were measured and the CMC determined.

In section 3.4 is given a comparison of the four different polymer systems that was investigated.

3.1 Homopolymers

The concentration dependence and the molar-mass dependence of the diffusion coefficient i aqueous solution of a series of P(MOx) homopolymers was measured, which can give information about the intermolecular interactions and the chain conformation.

3.1.1 Concentration dependence

The concentration dependence was measured with aminofluorescein (AF) labeled $P(MOx)_{22}$. The measurements were performed in an appropriate

buffer and the laser power was kept low in order to avoid bleaching. Figure 3.1 shows a typical correlation function for labeled $P(MOx)_{22}$ with a concentration of 2×10^{-6} M. From the fit of equation 2.7 (solid line), the number

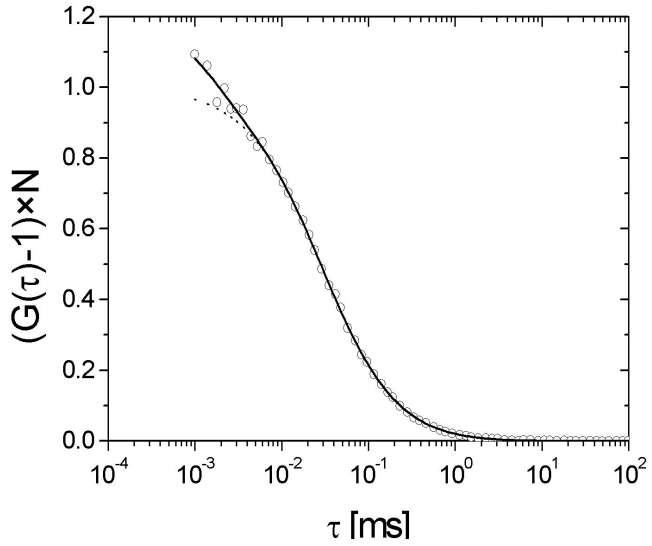

Figure 3.1 Correlation function of a solution of $P(MOx)_{22}$ with a polymer concentration of 2×10^{-6} M (○), (only every second point is shown). The solid line is a fit of equation 2.7 to the correlation function. The dashed line shows the diffusional part of the correlation function, i.e. the difference between this and the measured correlation function corresponds to the triplet contribution.

of fluorescence molecules on average present in the detection volume, N, is determined to be as low as 3.5 ± 0.1, which means that the concentration is suited for FCS measurements. The correlation function shown in figure 3.1 is normalized with the average number of fluorescence molecules in the focus, by plotting $(G(\tau) - 1) \times N$ rather than $G(\tau)$ (see equation 2.7). In this representation, correlation functions from solutions with different concentrations of fluorescence species can be directly compared. The diffusion time is 31 ± 1 μs, which corresponds to a diffusion coefficient $(2.5 \pm 0.1)\times10^{-10}$ m^2s^{-1}, found using equation 2.9. The dashed line in figure 3.1 shows the bare diffusional part of the fit. The difference between the dashed and the solid curve at $\tau \lesssim 5$ μs is due to the triplet decay. For a reliable determination of the diffusion time, it is important that the diffusion time and the triplet time are well separated and that the triplet fraction is low (see equation 2.6). This is the case in figure 3.1: The triplet time is 1.6 ± 0.2 μs and the triplet

fraction 0.18 ± 0.1. The triplet time is thus an order of magnitude lower than the diffusion time, and even though the triplet fraction is not negligible, it is possible to separate the diffusion from the triplet time.

The concentration dependence of the diffusion coefficient was measured in a range of 9×10^{-7} to 2×10^{-3} M (figure 3.2). The lower concentrations (9×10^{-7}

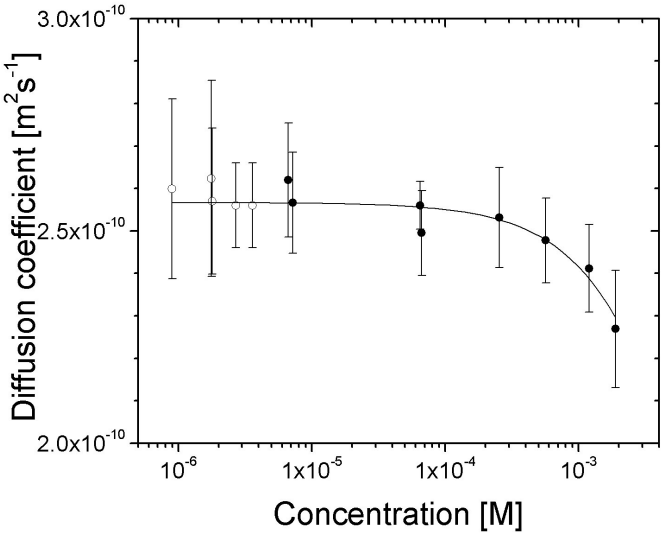

Figure 3.2 Concentration dependence of the diffusion coefficient of $P(MOx)_{22}$, labeled with aminofluorescein, in a buffer solution with pH = 9.0. The open circles are from solutions of only labeled polymer and the closed circles are solutions with both labeled and non-labeled polymers. The uncertainties are determined by repeating the measurement (at least ten times). The line is a fit of equation 3.1.

- 4×10^{-6} M) were measured on solutions of labeled polymer only (open circles). Higher concentrations were achieved with solutions containing both labeled and non-labeled polymers. The concentration of labeled polymers was kept in the interval 1×10^{-6} - 4×10^{-6} M. The concentration given in figure 3.2 is the total concentration of both labeled and non-labeled polymers. In this way, the amplitude of the correlation function was kept high (the amplitude is inversely proportional to the number of fluorescence particles in the volume, N). Varying the concentration of the labeled polymer did not have an influence on the measured diffusion coefficient. At concentrations below 8×10^{-4} M, the diffusion cofficient is constant within the limit of uncertainty of the FCS method. In contrast, above this value, the diffusion coefficient decreases significantly.

The solid line in figure 3.2 is a fit of the expression [31, 32]

$$D = D_0 (1 + k_c c) \tag{3.1}$$

where D_0 is the diffusion coefficient extrapolated to zero concentration, c is the concentration and k_c is related to the friction coefficient [32]. The decrease of D with concentration is due to intermolecular interactions of the polymers. When the concentration is increased, the polymers start to interact and thereby the diffusion coefficient is lowered.

From the fit, D_0 was determined to $(2.6 \pm 0.1) \times 10^{-10} \mathrm{m^2 s^{-1}}$. This value corresponds very well to the diffusion coefficient measured at concentrations below 8×10^{-4} M, which shows that it is sufficient to measure a single solution having a concentration below 8×10^{-4} M, in order to determine D_0.

From the fit, k_c was determined to (63 ± 27) l mole^{-1}. However, a quantitative evaluation of the k_c value determined from the fit in figure 3.2 is not meaningful. This value of k_c is not necessarily the value for non-labeled $P(MOx)_{22}$ since the concentration dependence was established using solutions containing both labeled and non-labeled polymers, and an influence of the fluorescence dye on the interactions between the polymers cannot be excluded.

3.1.2 Molar mass dependence

The dependence of the diffusion coefficient on the degree of polymerization was established using solutions of labeled polymers in aqueous solutions at concentrations below 10^{-6} M. Figure 3.3 shows FCS correlation functions of two aqueous solutions of labeled homopolymers with different degree of polymerization. The two polymers, $P(MOx)_{13}$ and $P(MOx)_{60}$, have a concentration of 9×10^{-7} and 3×10^{-7} M, respectively. Both polymer concentrations are well below 8×10^{-4} M, and the measured diffusion coefficients thus correspond to D_0. With increasing degree of polymerization, the decay is shifted to slightly higher times, as expected. This means, that the diffusion time increases with increasing degree of polymerization, i.e. the diffusion coefficient decreases and the hydrodynamic radius increases.

The diffusion coefficients of all four TRITC labeled homopolymers are given in figure 3.4. The range of the degree of polymerization is rather narrow (between 13 and 60 monomers) because longer homopolymers were not available. In spite of this limitation, we attempt to model the diffusion coefficient in dependence of the degree of polymerization. The full line in figure 3.4 is a fit,

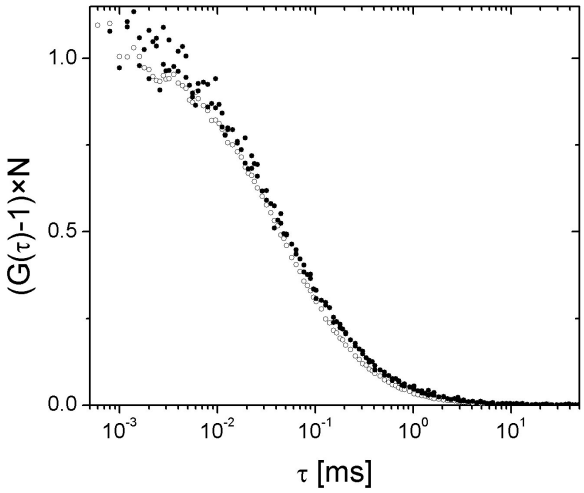

Figure 3.3 Correlation functions of $P(MOx)_{13}$ (○) and $P(MOx)_{60}$ (•) having concentrations of 9×10^{-7} and 3×10^{-7} M, respectively.

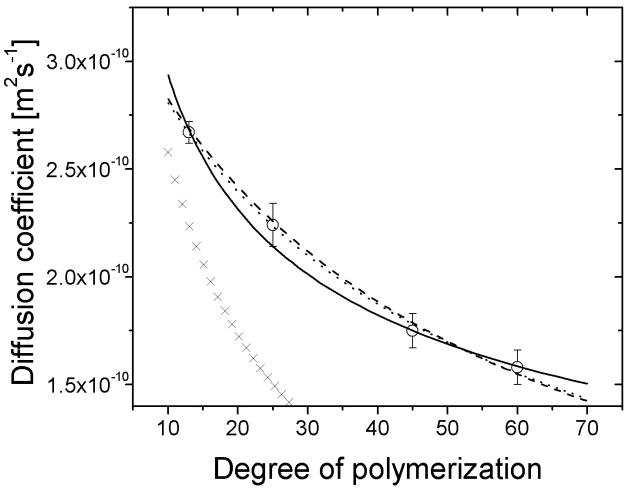

Figure 3.4 The diffusion coefficients measured for homopolymers with different degree of polymerization. The solid line is a fit assuming coils and the dotted and dashed lines are fits assuming rod-like particles. The uncertainty of the experimental data has been found by repeated measurements. (×) shows the diffusion coefficient for rod-like polymers, where the size has been estimated using CS Chem 3D [60].

assuming that the polymers have random coil conformation. The expected dependence is given by [89]

$$D \simeq \frac{k_B T}{\eta N_p^{\nu} b} \tag{3.2}$$

where k_B is Boltzmann's constant, T the absolute temperature, η the solvent viscosity, b the effective bond length, N_p is the degree of polymerization and the exponent ν is 0.5 for a theta-solvent and 0.59 in the good solvent limit [90]. Since water is a good solvent for 2-methyl-2-oxazoline, ν is expected to lie between these two values. The value of ν determined from the fit is 0.35 $\pm$ 0.02, thus much lower than the expected value.

Since the polymers studied have low degrees of polymerization, it is reasonable to assume a more rod-like conformation. The dashed line in figure 3.4 is a fit to the data, using the expression for rigid rod-like particles [89]

$$D = \frac{\ln\left(\frac{L}{w}\right)}{3\pi\eta L} k_B T \tag{3.3}$$

where L is the length of the polymer, and w is its width. The expression is valid for constant rod width; however figure 2.3 clearly shows that the dye is much wider than the P(MOx) part of the polymer. The length of the polymers has been assumed to be a linear function of the degree of polymerization, in addition to the length of the fluorescence dye

$$L = N_p \times a + d \tag{3.4}$$

where N_p is the degree of polymerization, a is the monomer length and d is the length of the fluorescence dye (including the piperazine spacer).

The fit has been carried out with a, d and w as free parameters. The outcome is shown in table 3.1 (*Fit 1*). The fit curve which is obtained, describes the experimental data well. However, the parameters are far from expectations: The value for the monomer length (0.1 nm) is shorter than estimated with the modelling software CS Chem 3D [60], which was 0.37-0.38 nm. Also the uncertainties from the fit are very large (larger than the values).

The fit was thus repeated with the monomer length kept fixed at 0.37 nm (dashed line in figure 3.4), shown in table 3.1 as *Fit 2*. However, the result values for w and d have not improved: w is now 2×10^{-5} nm, which is not realistic because it is much lower than the Bohr radius of 5×10^{-2} nm [91].

The values of a, w and d has been estimated using CS Chem 3D [60] (values given in table 3.4). The diffusion coefficient was calculated using equation

Table 3.1 *Fit 1* gives the values determined by the fit shown in figure 3.4 with all parameters left free (dotted line). *Fit 2* gives the values for a fit where a has been kept constant at a value of 0.37 nm [60] (dashed line in figure 3.4. The estimates have been done using CS Chem 3D [60]

Parameter	*Fit 1*	*Fit 2*	Estimate
a	0.1±0.5 nm	0.37 nm	0.37 nm
w	0.3±6 nm	$(3\pm2)\times10^{-5}$ nm	0.29 / 0.8 nm [a]
d	2.6±44 nm	16±2 nm	1 nm

[a] For the polymer chain and fluorescence dye, respectively.

3.3 and is shown in figure 3.4 ($w = 0.29$ nm has been used). As it can be seen in the graph, the difference between the measured and calculated diffusion coefficient is rather large.

So neither the coil nor the rigid rod model give good descriptions of the concentration dependence of the diffusion coefficient, and no reasonable values of the polymer conformations and size are obtained. One problem might be that the range of the molar masses is narrow. Sukhishvili et al. measured the diffusion coefficients of fluorescence labeled poly(ethylene glycol) in aqueous solution, in a molar mass range of 2,200 - 30,500 g mole^{-1} (degree of polymerization in the range 48 - 693) and found the expected functionality $D \propto N_p^{-1/2}$ [92] (the homopolymers measured here are in the interval 1,205-5,220 g mole^{-1}). So it is possible to use FCS for these kinds of investigations, but a larger range in molar masses is probably necessary, because the influence of the fluorescence dye is higher for low molar masses.

3.1.3 Summary

We have established a procedure to perform FCS measurements on polymer solutions in a large concentration range by using fluorescence labeled polymers as tracers. When the polymer concentration is kept low ($\lesssim 10^{-4}$ M), the diffusion coefficient measured with FCS corresponds to D_0 and can thereby be determined with a single measurement, instead of measuring a large concentration range.

It was possible to determine the dependence of the diffusion coefficient on degree of polymerization, even for a small range in degree of polymerization. Attempts to fit the dependence of the diffusion coefficient was made, assuming both coil and rod-like particles. None of the models gave reasonable

results, which is likely due to the influence of the fluorescence dye, which could be expected to be large for low molecular mass.

The measurements showed that TRITC is a suitable dye for FCS measurements. No aggregates were detected, which might have been caused by the fluorescence dye. When determining the CMC of an aggregating system, it is very important to be able to exclude dye aggregation as the driving force.

3.2 Diblock copolymers in aqueous solution

The aggregation behavior of P[(MOx)(NOx)] diblock copolymers in aqueous solution was investigated using fluorescence correlation spectroscopy (FCS), photon correlation spectroscopy (PCS) and small-angle neutron scattering (SANS). We expected solutions of single, dissolved polymers (unimers) at low concentration. Above the critical micelle concentration (CMC), they are expected to coexist with micelles of the core-shell type. It was our aim to the determine the CMC and to characterize the unimers and micelles.

The concentration dependence of the diffusion coefficient was measured with FCS at room temperature, again using labeled diblock copolymers as tracers in solutions of the identical non-labeled diblock copolymers. In this way, a large concentration range could be covered, keeping the concentration of labeled polymers at a minimum. Both labeled unimers and, above a certain concentration, micelles were detected, however, the size of the apparent micelles was much larger than the estimated contour length of the polymers. Temperature-resolved PCS experiments revealed that these large micelles are non-equilibrium aggregates, which could be annealed by heating the solutions (temperature variation was not possible with the FCS setup used). Non-equilibrium aggregates could also be characterized with SANS. Using annealed solutions, the hydrodynamic radius of the equilibrium micelles as well as the critical micelle concentration (CMC) could be determined using FCS at room temperature. The hydrodynamic radius of these equilibrium micelles determined by FCS and PCS coincide very well.

Modelling the relative amplitude of the FCS decay due to micelles determined by FCS as a function of concentration was attempted and showed, that the aggregation process is much more complex than the closed association model, when tracers are involved.

3.2.1 Non-equilibrium aggregates

Figure 3.5 shows two correlation functions from measurements on P[$(NOx)_{10}$-$(MOx)_{32}$]. The polymers had been prepared at room temperature. The correlation functions of a solution of 2×10^{-8} M labeled polymers can be described with a fit of equation 2.11, assuming a single diffusing component ($k = 1$). From the fit, the diffusion coefficient is determined to $(1.9 \pm 0.1)\times10^{-10}$ m^2s^{-1}. The resulting hydrodynamic radius, $r_H = 1.3 \pm 0.1$ nm, is close to the hydrodynamic radius of a homopolymer of similar degree of

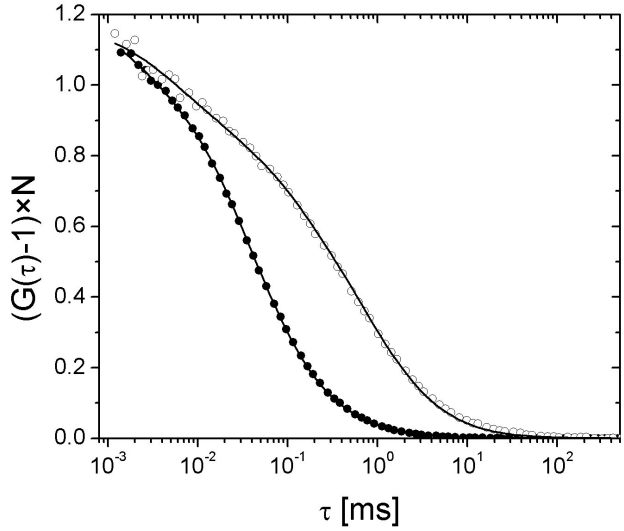

Figure 3.5 FCS correlation curves P[$(NOx)_{10}(MOx)_{32}$]. (•) 2×10^{-8} M solution of labeled polymers, (○) solution of 8×10^{-8} M labeled polymer and 9×10^{-3} M non-labeled polymers. The lines are a fit of equation 2.11 assuming a one and two species, respectively.

polymerization, $r_H = 1.4 \pm 0.1$ nm for $P(MOx)_{45}$, and this decay is therefore attributed to unimer diffusion.

The correlation function of a solution of 8×10^{-8} M of labeled polymers and 9×10^{-3} M of non-labeled polymers has a different shape, compared to the correlation function described above: An additional slower decay is observed (figure 3.5). The small difference in concentration of the labeled polymers is not expected to have a influence on the diffusion coefficient, since the concentrations are kept below 8×10^{-4} M (see section 3.1.1). The line is a fit of equation 2.11, assuming a unimer-micelle system (k=2). The two diffusion coefficients extracted for the fit of the fast and slow diffusional process are $(8 \pm 2)\times10^{-11}$ m^2s^{-1} and $(7 \pm 1)\times10^{-12}$ m^2s^{-1} respectively. These values correspond to hydrodynamic radii of 3.1 ± 0.8 nm for the fast and 35 ± 5 nm for the slow diffusional process.

The concentration dependence of the diffusion coefficients is shown in figure 3.6. With solutions of labeled polymers, only one diffusional process could be observed (see figure 3.5). The diffusion coefficient averaged over the values from labeled polymers is determined to $(1.8 \pm 0.2)\times10^{-10}$ m^2s^{-1}, which corresponds to a hydrodynamic radius of 1.4 ± 0.2 nm. This corresponds very

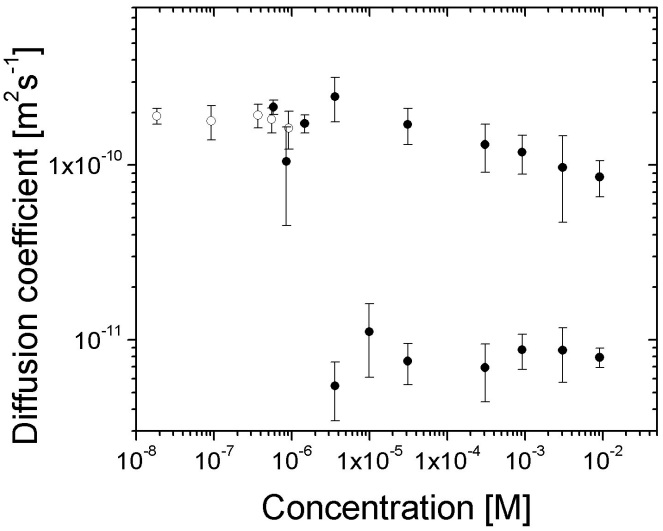

Figure 3.6 The concentration dependence of the diffusion coefficient of $P[(NOx)_{10}(MOx)_{32}]$ in solution with $P[(NOx)_{10}(MOx)_{32}]$-TRITC measured with FCS. The open and closed symbols denote measurements on solutions with labeled polymers only and solutions containing labeled and non-labeled polymers, respectively. The error bars have been determined by multiple measurements.

well with the hydrodynamic radius of a homopolymer with a similar degree of polymerization. The slow diffusional process, due to aggregates, is only observed when non-labeled polymers are added at a concentration higher than 2×10^{-6} M. The fast diffusional process is still present with its diffusion coefficient decreasing slightly with increasing concentration, as expected from the concentration dependence of the homopolymers (section 3.1.1). The average diffusion coefficient of the slow diffusional process is approximately $(8 \pm 2)\times10^{-12}$ m^2s^{-1}, which corresponds to a hydrodynamic radius of 31 $\pm$ 7 nm. This is larger than the contour length of $P[(NOx)_{10}(MOx)_{32}]$ which is estimated to be $\simeq$16 nm [60]. This discrepancy indicates that the aggregates formed cannot be spherical core-shell micelles, since this would imply that the polymers are stretched to twice their contour length.

In order to investigate the stability of these aggregates, temperature-resolved PCS experiments were carried out on solutions of non-labeled polymers above the CMC. An example of a heating and cooling run on $P[(NOx)_{10}(MOx)_{32}]$ is shown in figure 3.7. Each measurement lasted 30 minutes, and between the measurements, there was 30 minutes waiting time for thermal equilibrium.

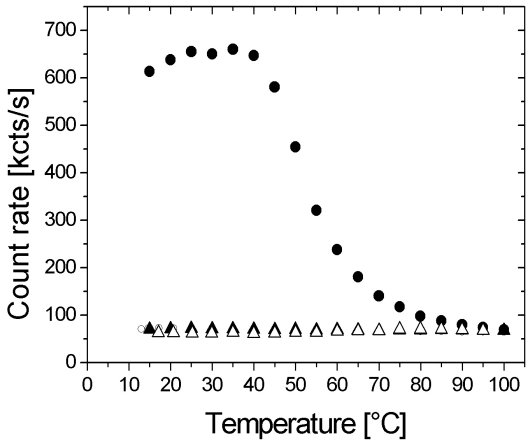

Figure 3.7 The intensity of the scattered light as a function of temperature, for a 3×10^{-3} M solution of non-labeled $P[(NOx)_{10}(MOx)_{32}]$. The circles and triangles denote the first and second heating/cooling cycle, and closed and open symbols denote heating and cooling, respectively.

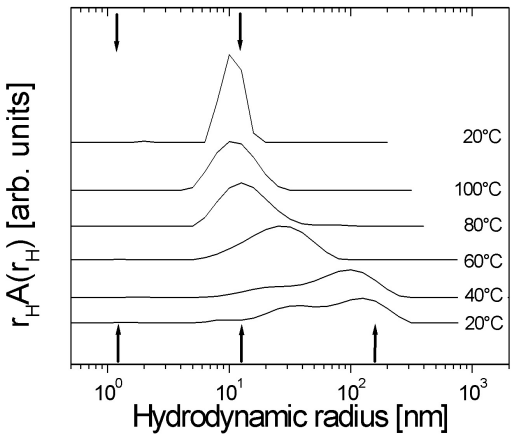

Figure 3.8 The distribution of hydrodynamic radii from PCS on a solution of non-labeled $P[(NOx)_{10}(MOx)_{32}]$ at a concentration of 3×10^{-3} M at different temperatures. The five lower curves were taken during the first heating cycle and the uppermost distribution at 20°C after cooling the sample. The arrows indicate the hydrodynamic radii determined with FCS (correlation functions are shown in figure 3.9) at room temperature on an annealed sample (top) and a non-annealed sample (bottom).

These experiments shows that at temperatures below 40°C, the scattered intensity is nearly constant, whereas it decreases at higher temperatures. Upon subsequent cooling, the scattering intensity does not increase to the same level as before, but remains constant at a low level also during further heating and cooling cycles. This shows that heating the sample leads to irreversible changes. As the scattering intensity is proportional to the molar mass and to the concentration of the objects scattering the light [13], the decrease of the intensity upon heating can be attributed to the dissolution of particles in the solution.

More specific information about these changes can be deduced from the corresponding size distributions (figure 3.8). They were obtained by indirect Laplace transformation on the corresponding correlation functions. Initially, at 20°C, the distribution is very broad, ranging from 10 nm to $\sim$ 300 nm, having its center of gravity at $\sim$ 70 nm. Up to 40°C, almost no change in the distribution is observed, but heating to 60°C leads to significant changes: Firstly, it gets narrower and, secondly, it moves towards smaller hydrodynamic radii. This trend continues up to 100°C. At 100°C, the PCS distribution is centered around $\sim$ 11 nm. The distribution at 20°C after subsequent cooling is very similar to the one at 100°C.

In order to characterize the kinetics, a solution was prepared at room temperature at a concentration of 1.7×10^{-2} M, and was kept at 40°C for a period of 24 hours. PCS measurements with a duration of 5 minutes showed that even after 24 hours, the scattered intensity kept decreasing, i.e. equilibrium was not reached. Equilibrium seems to be reached faster, when the temperature is increased; in the temperature scan shown in figure 3.7, equilibrium was reached within 12 hours (the time difference between the measurement at 40°C and 100 °C). The results indicate that the distributions in figure 3.8 are not in equilibrium, because they were measured at higher heating rate. Only at 100°C, the system appears to be in equilibrium.

Similar behavior upon heating has previously been observed with chemically different diblock copolymer solutions in selective solvents [93]. Poly[styrene-*b*-(ethylene-*co*-propylene)] dissolved in decane also showed large aggregates at low temperatures, which disappeared upon heating and did not reappear when the sample was cooled. This was attributed to the presence of non-equilibrium aggregates. The authors suggested that if the insoluble blocks are strongly bound, formation of equilibrium micelles may be very slow, and non-equilibrium aggregates are observed. Also other authors report that upon direct dissolution of diblock copolymers in selective solvents, the formation of equilibrium micelles may be very slow, especially if one block is in the glassy or crystalline state [35, 39].

The diffusion coefficients shown in figure 3.6 were calculated on the basis of a two-component unimer-micelle system. However, the light scattering results imply that a third component is present, namely large non-equilibrium aggregates, which vanished upon heating. In addition, the fit to the FCS correlation curve is not good above $\simeq$ 2 ms (see figure 3.5). The effect of heating on the FCS correlation functions is shown in figure 3.9. The

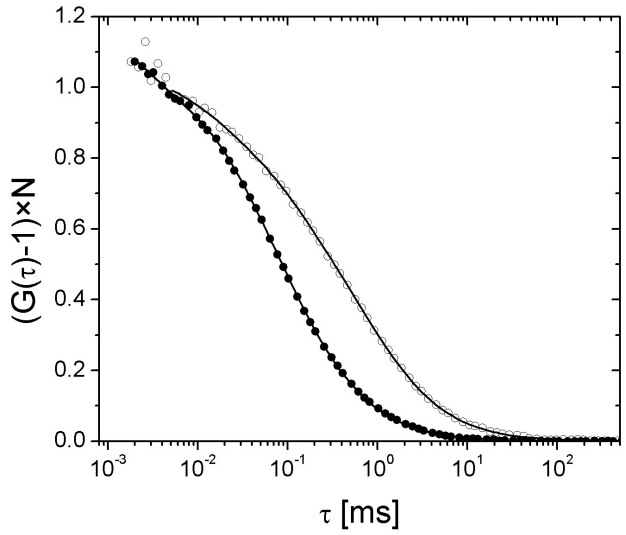

Figure 3.9 The correlation functions for two solutions of P[$(NOx)_{10}(MOx)_{32}$] measured with FCS. (•) Solution containing labeled (6×10^{-8} M) and annealed non-labeled polymers (2×10^{-3} M). (○) Solution of labeled (8×10^{-8} M) and non-labeled polymers, which was not annealed (9×10^{-3} M). The lines are fits to equation 2.11 with $k = 2$ and 3, respectively.

correlation function of the annealed solution decays more rapidly than the non-annealed one. This is in agreement with the PCS results, which showed that upon annealing, non-equilibrium aggregates vanish and do not reappear upon cooling. The resulting hydrodynamic radii are compiled in table 3.2 and are compared with values from PCS. They are also shown as arrows in figure 3.8 (bottom). The hydrodynamic radius of the micelles, $r_H^{micelles}$, in annealed samples is determined to $\sim$ 12 nm, which is lower than the contour length and thus a realistic value for the aggregates. The hydrodynamic radius of the non-equilibrium aggregates determined with PCS has been determined by averaging over several measurements between 20 and 40°C. The values determined by the two methods for the hydrodynamic radius for micelles

Table 3.2 Comparison of hydrodynamic radii determined for P[$(NOx)_{10}$-$(MOx)_{32}$]with FCS and PCS.

Conc. [M]	Annealing	Method	r_H^{unimer} [nm]	$r_H^{micelle}$ [nm]	r_H^{nea} [nm] (a)
2×10^{-8} (b)	No	FCS	1.3 ± 0.1	-	-
9×10^{-3} (c)	No	FCS	1.2 ± 0.5	13 ± 2	140 ± 20
3×10^{-3}	No	PCS	-	12 ± 3	122 ± 19
2×10^{-3} (c)	Yes	FCS	1.3 ± 0.1	12.3 ± 0.6	-
3×10^{-3}	Yes	PCS	-	12.0 ± 0.4	-

(a) nea stands for non-equilibrium aggregates. (b) PCS was not possible at this low concentration. (c) Solution contains labeled and non-labeled P[$(NOx)_{10}(MOx)_{32}$].

and non-equilibrium aggregates correspond very well. With PCS, it was not possible to determine the hydrodynamic radius of the unimers.

Small-angle neutron scattering

Small-angle neutron scattering on a very similar sample allowed us to verify the simultaneous presence of micelles and non-equilibrium aggregates, in addition to characterize their shape. In order to get information on the overall shape and to compare with FCS and PCS, the contrast was maximized by using D_2O (see section 2.4.1). The scattering functions for the solution before and after annealing are shown in figure 3.10. Significant changes upon annealing are seen.

The corresponding pair distance distribution functions, $p(r)$, are shown in figure 3.11. The $p(r)$ from the non-annealed sample, shows two peaks. The first peak has the maximum at 7.5 nm and the second peak has a maximum at 24 nm. For the annealed sample, only one maximum is present in the $p(r)$, at 6.6 nm, and the $p(r)$-function is dominantly bell-shaped, suggesting that the aggregates consists of spherical micelles [26, 85]. The size and shape of the equilibrium micelles are thus unchanged by the annealing.

The micellar hydrodynamic radius of annealed micelles of P[$(NOx)_{10}$-$(MOx)_{32}$], determined with FCS and PCS, is approximately 12 nm, whereas the radius determined with SANS is 6.6 nm. The radius from the $p(r)$ is presumably not the size of the entire micelle, as the outer corona has a much lower density and thereby lower contrast with respect to D_2O [26].

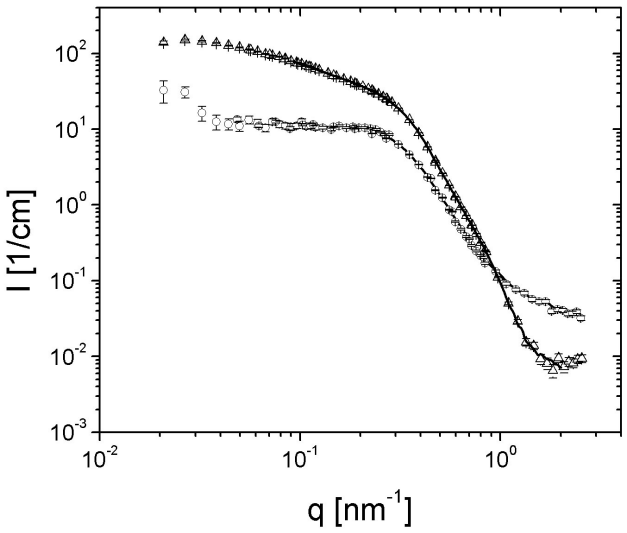

Figure 3.10 SANS intensity curves from a solution of 0.014 M non-labeled P[(NOx)$_6$(MOx)$_{30}$] in D_2O before (△) and after annealing (○). The lines are fits determined with GIFT.

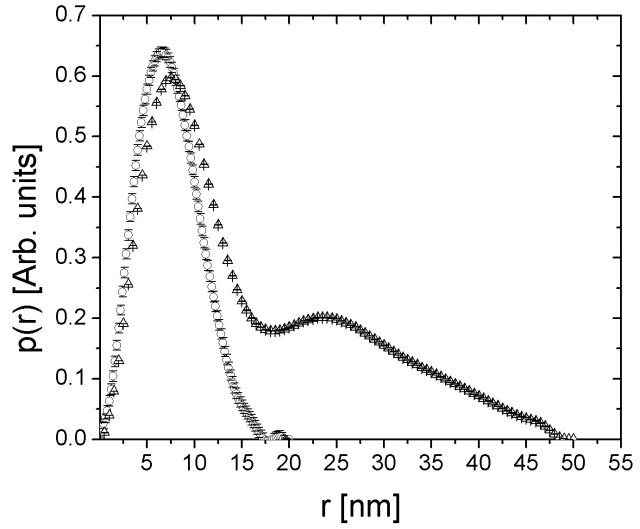

Figure 3.11 The corresponding $p(r)$ functions determined using GIFT. Same symbols as in figure 3.10.

Summary

When the diblock copolymers were dissolved directly in water, non-equilibrium aggregates were detected with both FCS, PCS and SANS. The non-equilibrium micelles could be detected in coexistence with equilibrium micelles. With FCS it was possible to detect labeled unimers, equilibrium micelles and non-equilibrium aggregates simultaneously. The non-equilibrium aggregates could be annealed by heating the sample. After annealing, equilibrium micelles could be detected with PCS and SANS. With FCS labeled unimers and equilibrium micelles could be detected.

3.2.2 Determination of the CMC with polymeric tracer

The CMC was determined from FCS measurements on a concentration series of annealed solutions. The FCS correlation functions of $P[(NOx)_{10}(MOx)_{32}]$ are shown in figure 3.12 for several concentrations in the range 8×10^{-8} - 3×10^{-3} M, i.e. nearly five orders of magnitude. For solution with concentra-

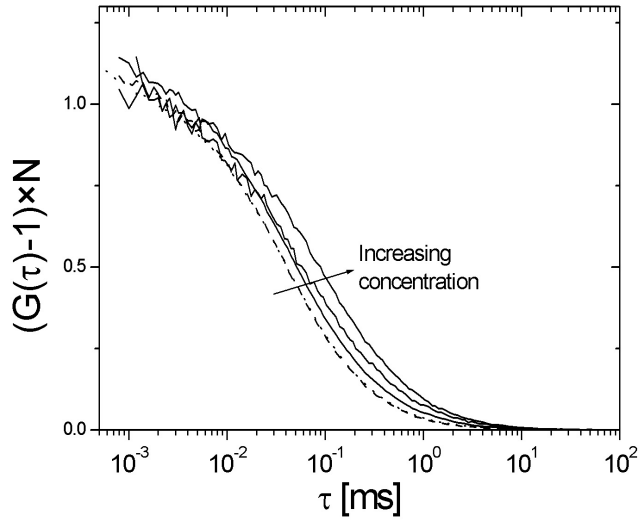

Figure 3.12 FCS correlation functions for five different concentrations of $P[(NOx)_{10}(MOx)_{32}]$. The concentrations are 8×10^{-8} M (dashed line), 3×10^{-6} M (dotted line), 3×10^{-5} M, 3×10^{-4} M and 3×10^{-3} M. The solution of the lowest concentration contains labeled polymers only, whereas the others contain both labeled and non-labeled polymers. The dotted and dashed line are difficult to separate, since the curves are almost identical.

tions of 3×10^{-6} M and below, the curves can be fitted with a single diffusion decay, corresponding to unimer diffusion. For solutions with a concentration of 3×10^{-5} M and above, the curves can only be fitted satisfactorily with two diffusional decays ($k = 2$ in equation 2.11). The diffusion coefficient of the slow decay corresponds very well with the one from PCS on annealed solutions, and we therefore attribute this additional slower diffusional decay to micelle diffusion. We assign the appearance of this slower diffusional decay to the CMC.

In order to precisely determined the CMC, the concentration dependence of the diffusion coefficients of both diblock copolymers was measured in smaller

steps. The results are shown in figure 3.13, both for P[$(MOx)_{40}(NOx)_7$], labeled at the hydrophobic end, and P[$(NOx)_{10}(MOx)_{32}$], labeled at the hydrophilic end. The CMC's are determined from the appearance of the slow diffusional decay. The relative amplitude of the slow decay, determined from the fits, increases above the CMC from zero to 0.5 at concentrations of 1.5×10^{-2} M and 3×10^{-3} M for P[$(MOx)_{40}(NOx)_7$] and P[$(NOx)_{10}(MOx)_{32}$], respectively (see figure 3.14). This means that in the entire concentration range, even above the CMC, unimers are present. This is further discussed in section 3.2.3. The CMC's are found at $(8\pm2)\times10^{-6}$ M and $(2\pm1)\times10^{-5}$ M for P[$(MOx)_{40}(NOx)_7$] and P[$(NOx)_{10}(MOx)_{32}$], respectively.

The results from measurements from FCS and PCS on the diblock copolymers are compiled in table 3.3.

Table 3.3 Results from FCS and PCS on annealed solutions of P[$(MOx)_{40}$-$(NOx)_7$] and P[$(NOx)_{10}(MOx)_{32}$], which have the fluorescence label attached to the hydrophobic and hydrophilic end, respectively.

Polymer	Method	r_H^{unimer} [nm]	$r_H^{micelle}$ [nm]	CMC [M]
P[$(MOx)_{40}(NOx)_7$]	FCS	1.4 ± 0.4	13 ± 2	$(8\pm2)\times10^{-6}$
	PCS	-	11.9 ± 0.7	-
P[$(NOx)_{10}(MOx)_{32}$]	FCS	1.3 ± 0.2	11.3 ± 0.9	$(2\pm1)\times10^{-5}$
	PCS	-	11.5 ± 0.9	-

The hydrodynamic radius of the unimers, r_H^{unimer}, determined with FCS, for the two diblock copolymers are very similar. The hydrodynamic radius also corresponds very well with the one of the homopolymers. It was not possible to determine the hydrodynamic radius of the unimers with PCS.

The micellar hydrodynamics radii, $r_H^{micelles}$, determined with FCS and PCS, coincide very well. This shows that when a fluorescence dye is attached to the polymers, it does not have a measurable influence on the size of the formed micelles (though it should be expected to have an influence on the unimer size). The hydrodynamic radii of the two diblock copolymers are very similar. The hydrodynamic radius is lower than the calculated contour length of the polymers ($\sim$ 16-17 nm for the two polymers), showing that the polymers are not completely stretched in the micelles, as expected.

The CMC's of the P[(MOx)(NOx)] diblock copolymers are in the same range as for chemically different, low molecular mass, non-ionic block copolymers, 10^{-8} - 10^{-2} M, depending on the chemical composition (see table 1.1). The CMC's of the two diblock copolymers are very similar to each othe, which is expected since the degrees of polymerization is similar. It was not possible to

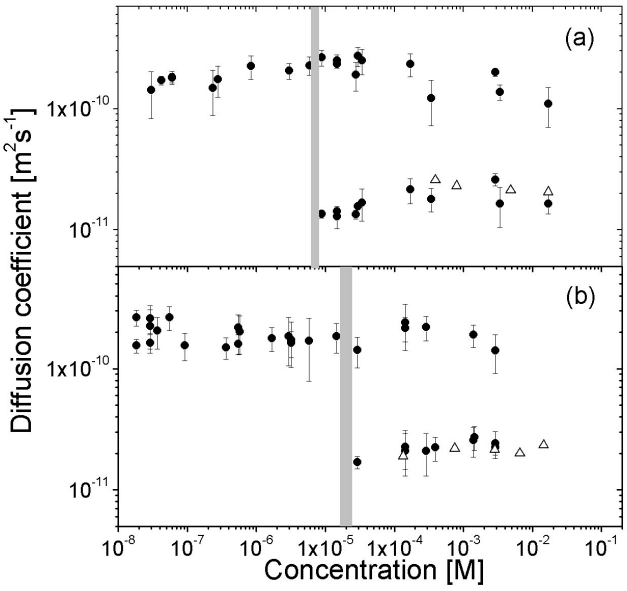

Figure 3.13 The concentration dependence of the diffusion coefficients measured with FCS (•) and PCS (△) for solutions of $P[(MOx)_{40}(NOx)_7]$ (a) and $P[(NOx)_{10}$-$(MOx)_{32}]$ (b).

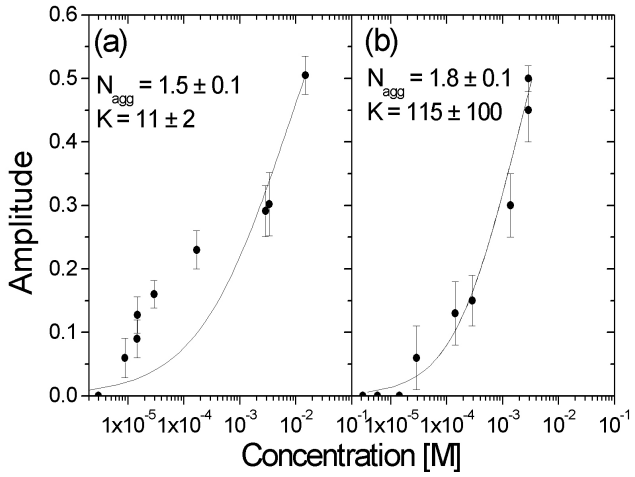

Figure 3.14 The relative amplitude of the slow decay in the FCS correlation curved (due to micelles) as a function of concentration for the two diblock copolymers $P[(MOx)_{40}(NOx)_7]$ (a) and $P[(NOx)_{10}(MOx)_{32}]$ (b). The lines are fits of equation 3.9, which are discussed in section 3.2.3.

determine the CMC for any of the two polymers using PCS, since the detection level of the PCS setup was almost a factor of ten above the CMC. The key difference between the two diblock copolymers is the position of the fluorescence label, which is placed at the end of the hydrophobic block ($P[(MOx)_{40}$-$(NOx)_7]$) and on the hydrophilic block ($P[(NOx)_{10}(MOx)_{32}]$). The position of the label does not influence the CMC in these tracer experiments. This might be due to that the concentration of the labeled polymers is much lower than the total polymer concentration when the CMC has been reached (the concentration of labeled polymers was $\sim 10^{-8}$ M) so there are only very few labels per micelle, and the influence is therefore minimum.

The values determined with FCS ($r_H^{unimers}$, $r_H^{micelles}$ and CMC) and PCS ($r_H^{micelles}$) are very similar for the two diblock copolymers, which should also be expected, because of the very similar degrees of polymerization.

3.2.3 Model for the diblock copolymer aggregation

We now attempt to determine the aggregation number of the micelles. For this purpose, we evaluate the increase of the amplitudes of the slow diffusional decay (micelles) with polymer concentration (figure 3.14).

If it is assumed that the fluorescence properties of the dye are the same when the labeled polymer is dissolved as a unimer or when it is part of a micelle then the amplitude of the slow decay in the FCS correlation curve is equal to the fraction of labeled polymers present in micelles.

If it is further assumed that the dye on the labeled polymers does not influence the aggregation behavior, the concentration dependence of the fraction of micelles can be modelled by the closed-association model [1, 13]. The closed-association model has previously been used to describe the aggregation of amphiphilic polymer systems [30, 94, 95, 96]. An equilibrium between unimers and micelles, with one dominating aggregation number, N_{agg}, is assumed:

$$N_{agg} \text{ unimer} \rightleftarrows \text{micelle} \tag{3.5}$$

The equilibrium constant, K, then reads

$$K = \frac{[M]}{[U]^{N_{agg}}} \tag{3.6}$$

where $[M]$ is the concentration of micelles and $[U]$ is the concentration of unimers. Because the concentrations of unimers and micelles are unknown

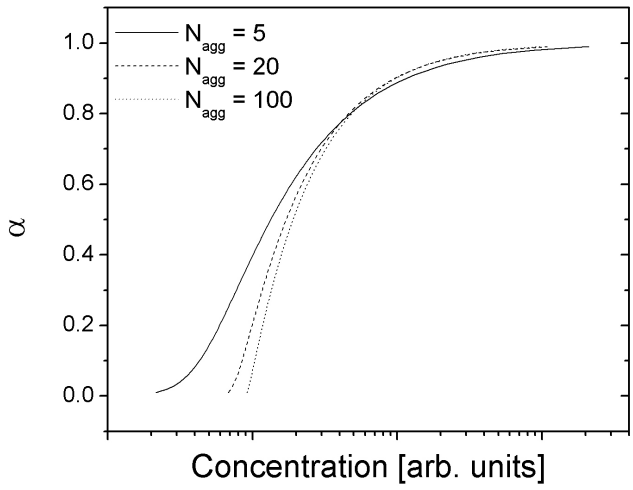

Figure 3.15 The fraction of polymers present in micelles, α, as function of concentration as derived in equation 3.9 for three different aggregation numbers. The equilibrium constant has been set to $K = 1$ in all three curves. Note that the concentration has been scaled, so that the curves are in the same range.

and only the total polymer concentration is known, they must be expressed in terms of the total polymer concentration

$$[M] = \frac{\alpha c_t}{N_{agg}} \tag{3.7}$$

where α is the fraction of polymers present as micelles and c_t is the total polymer concentration. Likewise, the unimer concentration can be written as

$$[U] = (1 - \alpha)\, c_t \tag{3.8}$$

In equations 3.7 and 3.8, it is assumed that all polymers are either present as unimers or micelles. Combining them with equation 3.6 leads to

$$K = \frac{\alpha c_t}{N_{agg}\left[(1 - \alpha)\, c_t\right]^{N_{agg}}} \tag{3.9}$$

This relation between c_t and α holds under the assumption that N_{agg} and K are kept constant. Figure 3.15 shows the concentration dependence of α for three different aggregation numbers. It can be seen that α increases with

concentration, as expected. Also, if the aggregation number is decreased, α increases more slowly.

For the diblock copolymers, the amplitude of the slow decay a as function of the concentration was determined from the fits to the FCS correlation functions (figure 3.14). The amplitude increases with concentration, and if it is assumed that the amplitude of the slow decay is equal to the fraction of micelles, it follows the prediction of equation 3.9. The lines in the graphs are fits of equation 3.9. For P[$(NOx)_{10}(MOx)_{32}$] (figure 3.14B), the fit is fairly good. The value found for the aggregation number, $N_{agg} = 1.8$, however, is not realistic, because two polymers cannot give the volume of one micelle. The fit to the data from P[$(MOx)_{40}(NOx)_7$] is not good, especially at low concentrations. The aggregation number found here is $N_{agg} = 1.5$, i.e. also too low.

The different behavior of the concentration dependence of the amplitude of the slow decay for the two polymers indicates that the position of the fluorescence dye alters the aggregation behavior. This effect was not seen in in the determination of the hydrodynamic radius and the CMC and might be caused by a change in amphiphilicty of the polymer induced by the fluorescence dye.

One of the assumptions of the model was that the labeled polymers have the same aggregation behavior as the non-labeled polymers. This is not necessarily the case, since different end-groups can have a large effect on the behavior of low molar mass polymers [97, 98]. It would then be a coupled equilibrium, where the first step is the formation of micelles, and the second step is an exchange of a labeled unimer with polymers in the micelle

$$\text{micelle} + \text{unimer}^* \rightleftarrows \text{micelle}^* + \text{unimer} \tag{3.10}$$

where the star means that it carries one label. The total number of micelles, $M_{total} = M + M^*$, is determined by the equilibrium shown in equation 3.5, under the assumption that a labeled polymer in a micelle does not disturb the initial equilibrium. The equilibrium constant for the exchange reaction, K_2, can be written as

$$K_2 = \frac{[M^*]\,[U]}{[U^*]\,[M]} \tag{3.11}$$

The concentration of labeled polymers is much lower than the concentration of non-labeled polymers, so it is safe to assume that a labeled micelle contains at most one labeled polymer. Then, the fraction of labeled unimers which are bound to a micelle reads

$$\alpha = \frac{[M^*]}{[U^*] + [M^*]} \tag{3.12}$$

The concentration of non-labeled polymers is accordingly

$$c_t = [U] + N_{agg} \times [M] + (N_{agg} - 1) \times [M^*] \tag{3.13}$$

and the concentration of labeled polymer reads

$$c_t^* = [U^*] + [M^*] \tag{3.14}$$

Combining these equations gives an expression for the fraction of labeled micelles

$$\alpha = \frac{c_t - [U] - N_{agg}\,[M]}{(N_{agg} - 1)\,c_t^*} \tag{3.15}$$

However, both $[U]$ and $[M]$ are unknown functions of the total concentration and so far it has not been possible to find a satisfactory solution for this problem.

We conclude that the attempt to describe the aggregation behavior of the P[(MOx)(NOx)] by the closed association model was not successful. This is probably because the fluorescence dye alters the aggregation behavior of the labeled polymers, and it must be described by a more complicated coupled equilibrium.

The aggregation number can in principle be determined from SANS in combination with contrast matching. If a D_2O/H_2O mixture is chosen such that only the micellar core is visible, the core size and thus the aggregation number can be estimated. Such work is currently in progress [99]. First results indicates a core radius of ~ 2.6 nm, which yields an aggregation number of $N_{agg} \sim 20$.

3.2.4 Determination of the CMC using a low molar mass tracer

The question arises if the use of labeled diblock copolymers as tracers in FCS is necessary or if the aggregation behavior can be characterized using commercially available fluorescence dyes as tracers in P[(MOx)(NOx)] solutions. Therefore a concentration series was measured, using Rh6G as a tracer in solution of non-labeled $P[(NOx)_{10}(MOx)_{32}]$. Rh6G was chosen because of its relatively low solubility in water (it is known to form dimers at concentrations above 10^{-5} M [100]) and its high solubility in polar organic solvents [100, 101, 102]. It is thus expected to be present in the micellar core. In this way, the micellar size and CMC, can be determined. A few FCS correlation

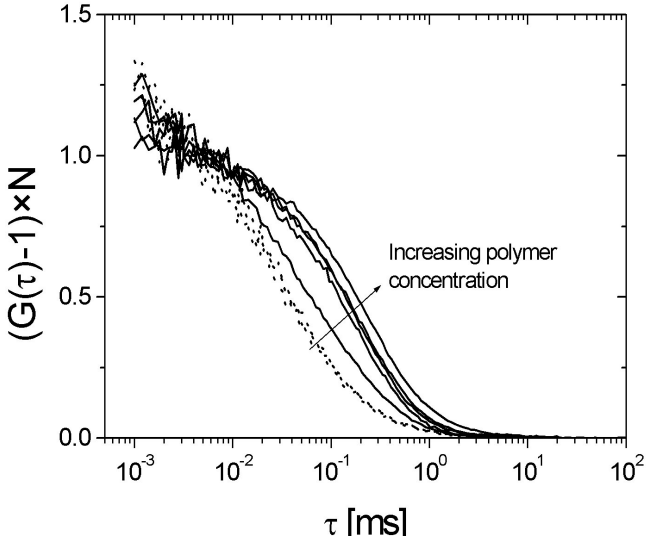

Figure 3.16 FCS correlation functions of solution of Rh6G and non-labeled $P[(NOx)_{10}(MOx)_{32}]$ at different polymer concentrations: 1.3×10^{-6}, 2.6×10^{-6}, 1.3×10^{-5}, 2.6×10^{-5}, 1.3×10^{-4}, 2.6×10^{-4}, 1.3×10^{-3} and 2.6×10^{-3} M. The concentration of Rh6G was 1×10^{-8} M in all experiments. The dotted and solid lines are from solutions with polymer concentrations below and above the CMC, respectively.

functions at different polymer concentrations (the concentration of Rh6G was kept constant in all experiments) are shown in figure 3.16. When the polymer concentration is kept below the previously measured CMC (the three correlation curves with dotted lines in figure 3.16), the correlation functions can be fitted very well with one diffusional process with diffusion coefficients similar to the one of Rh6G in aqueous solution. This means that at these concentrations, no micelles are formed, or at least, Rh6G is not attached to the micelles. When the polymer concentration is increased above 1.3×10^{-5} M, a change in the correlation functions can be observed. This indicates that the concentration is above the CMC and that the dye is present in the micelles. As the concentration is increased further, the diffusion decay in the correlation functions moves to longer correlation times, indicating a co-existence of Rh6G, unimers and micelles containing Rh6G. The correlation function can be described by a two-component system, in the same way as with labeled polymers as tracers.

The diffusion coefficients as a function of polymer concentration are shown

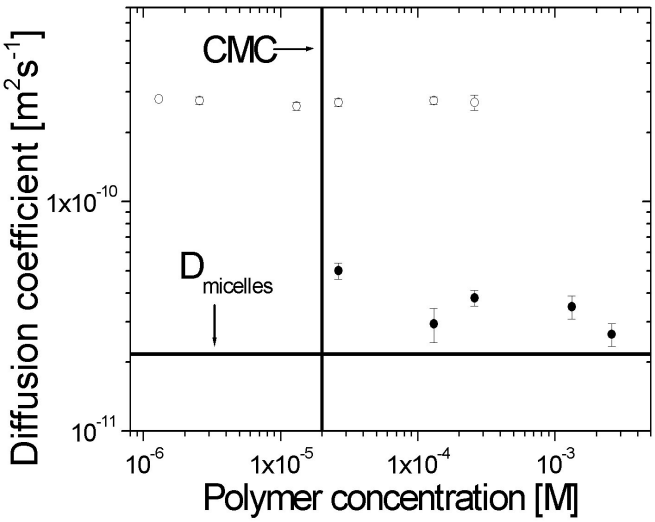

Figure 3.17 The concentration dependence of the diffusion coefficient in solutions of the polymer $P[(NOx)_{10}(MOx)_{32}]$ and Rh6G. The vertical line is the previously measured CMC and the horizontal line is the previously measured average diffusion coefficient for the micelles.

in figure 3.17. At concentrations above 2.6×10^{-4} M, the diffusion of the free dye could no longer be observed, which means that all the dye was bound to micelles. The horizontal line indicates the previously determined micellar diffusion coefficient, and the vertical line indicates the CMC, as determined with FCS using labeled polymers as tracers. The CMC-values coincide very well, regardless of which tracer was used.

The diffusion coefficient of the aggregates however, cannot be determined reliably with Rh6G tracers. A possible reason for this is that Rh6G is not water-insoluble enough to be tightly bound to the core of the micelle but may only be loosely attached to the corona. That could mean that the possibility for fast exchange between micelle and solution is increased and the determined diffusion coefficient is an average between the diffusion coefficients of the tracer in solution and attached to a micelle. The average diffusion coefficient can be written as [31]

$$\bar{D} = (1 - p_{\text{mic}})\, D_{\text{sol}} + p_{\text{mic}} D_{\text{mic}} \tag{3.16}$$

where D_{sol} and D_{mic} are the diffusion coefficients of the dye in solution and when attached to a micelle, respectively. p_{mic} denotes the probability of

finding the tracer attached to a micelle, if the dye properties do not change when a dye molecule joins a micelle. p_{mic} may also be regarded as the fraction of time that the dye is attached to a micelle. Since the diffusion coefficients of the fluorescence dye and the micelle are known, p_{mic} can be calculated. p_{mic} is 0.85 ± 0.02 and 0.98 ± 0.01 for the lowest and highest concentration above the CMC (2.6×10^{-5} M and 2.6×10^{-3} M), respectively. This shows that when the polymer concentration is increased (and thereby also the micelle concentration), the time fraction that Rh6G is attached to the micelles also increases. This effect was not observed, when the labeled polymer was used as tracer. That is most likely because the residence time of the labeled polymer in the micelle, is presumably much larger than the diffusion time of the micelles through the FCS detection volume (which is in the range 300 - 500 μs). For instance, the residence time for Pluronics systems (ABA triblock copolymers of ethylene oxide and propylene oxid) has been estimated to be below 1 ms [31, 103]. In the P[(MOx)(NOx)] system, it is likely that the residence time is even longer, because of the long side-chains of P(NOx) leading to high friction within the core of the micelle.

These experiments shows that using a commercially available, low molar mass fluorescence dye, it is possible to determine the CMC. In contrast, the hydrodynamic radii of the micelles cannot easily be determined, especially if the fluorescence dye has a relatively high solubility in water.

Even if the fluorescence dye is hardly soluble in the solution, it is not necessarily straightforward to determine the hydrodynamic radius of the aggregates with FCS. Loos et al. have measured the CMC of poly[(amylose)-*b*-(styrene)] diblock copolymers in THF, using rhodamine b, which is hardly soluble in THF, as tracer [48]. They were able to identify a very low CMC (in the range 1×10^{-7} - 1×10^{-6} M) and found aggregate sizes of $\sim$ 35 nm. PCS on the same polymer gave an aggregate size of $\sim$ 50 nm. The hydrodynamic radius from FCS, using a fluorescence dye as tracer, was thus underestimated significantly.

Schuch et al. measured the CMC of poly[(isobutylene)-*b*-(methacrylic acid)] with different degrees of polymerization in aqueous solution, using a fluorescence bodipy dye with a C_{16} fatty acid attached in order to make it more hydrophobic [45]. The micellar size was found to increase with concentration and reached a plateau. They assigned the beginning of the increase to the CMC, giving a value in the range of 1×10^{-8} - 4×10^{-8} M (see also table 1.1).

Hink et. al. [49] measured the hydrodynamic radius of different micellar solutions with FCS, using two different, fluorescence labeled phospholipids as tracers, which were labeled at the hydrophilic or the hydrophobic part.

They observed that the hydrodynamic radius measured with the tracer was in general higher than the previously reported values without tracers. They also observed that when the tracer was labeled on the hydrophobic end, the increase in hydrodynamic radius was larger than when the tracer was labeled on the hydrophilic end. PCS experiments confirmed this change in hydrodynamic radius, when the tracer was introduced. This stands in strong contrast to our results shown in figure 3.13: In the P[(MOx)(NOx)] system, there is no significant change of the micellar hydrodynamic radius, when determined with the polymeric tracer (FCS) and without a tracer (PCS). This is most likely due to the fact, that in our system, the polymer and the tracer are very similar.

3.2.5 Summary

In this section, the aggregation behavior of P[(MOx)(NOx)] diblock copolymers was investigated, using FCS in combination with PCS and SANS. It was shown that when dissolving the diblock copolymers in water at room temperature, they form large non-equilibrium aggregates. The measurements show a coexistence of equilibrium micelles and non-equilibrium aggregates were present. The non-equilibrium aggregates can be annealed by heating the sample and annealing did not affect the equilibrium micelles.

The CMC of equilibrated solutions of diblock copolymers could be determined by measuring the concentration dependence of the diffusion coefficient of annealed samples with FCS, using labeled polymers as tracers in solutions of non-labeled polymers. The micellar hydrodynamic radius was very similar for the two diblock copolymer systems, showing that the influence of the position of the fluorescence dye does not have an influence on the micellar size.

The concentration dependence of the diffusion coefficients of the two diblock copolymers was also measured using PCS, but here the CMC was approximately a factor of 10 below the detection limit of the setup used. The micellar hydrodynamic radii measured with FCS and PCS coincide very well.

In an attempt to determine the aggregation number, the concentration-dependent fraction of polymers present as micelles, determined by FCS, was modelled by the closed-association model. The model fitted the data well, but the extracted values for the aggregation number is very low. The discrepancy between the determined and expected values probably arises because the labeled polymers do not have the same aggregation behavior as the non-labeled polymers, which is assumed in the model. An attempt was made

to model the aggregation behavior as a coupled equilibrium, but a quantitatively evaluation could no be performed, because the fraction of non-labeled polymers present as unimers and as micelles is not known.

Finally, it was tested, if the same aggregation behavior could be determined with FCS, when a low molar mass tracer was used as a tracer instead of labeled polymers. Therefore the concentration dependence of the diffusion coefficient of one of the diblock copolymers was measured using the commercially fluorescence dye Rh6G as a tracer. In these experiments, the value of the CMC could be reproduced, but the hydrodynamic radius of the micelles was smaller than the previously determined value, probably due the fast exchange of the dye between micelle and solution. This shows the advantage of using fluorescence labeled polymers as tracers in FCS experiment

3.3 Other architectures

In order to investigate the effect of the polymer architecture, two other copolymer types were investigated by FCS wit respect to the diffusion coefficients and the CMC. The two architectures investigated are triblock and random copolymers, which consist of the same monomers as the diblock copolymers described above.

3.3.1 Triblock copolymers

Two triblock copolymers, both of the ABA type, where A and B denote the water-soluble and water-insoluble parts, respectively, were investigated. The two polymers have the same degree of polymerization for the hydrophobic block, but the degree of polymerization of the hydrophilic block is varied. The diffusion coefficient was measured and the CMC was determined. As for the diblock copolymers we expect that these types of polymers will form spherical micelles, but with different chain conformation because both ends of the middle block need to be at the surface of the micellar core.

Initially we also wanted to investigate the aggregation behavior of BAB triblock copolymers in aqueous solution, i.e. having a water-soluble middle block. These types of triblock copolymers have been reported to form two different kinds of aggregates [104, 16]: At low concentration, they form so-called flowers, where the A block forms a loop (and both B blocks are in the same micelle core). At higher concentrations, so-called animals are formed, where the A block forms a bridge between two micelles (the B blocks are part of two different micelles). Two polymers were supplied, having the compositions P[$(NOx)_7(MOx)_{54}(NOx)_7$] and P[$(NOx)_{10}(MOx)_{40}(NOx)_{10}$], but unfortunately none of these triblock copolymers could be dissolved in water. One reason could be that loosening of the two P(NOx) blocks from the same polymer is a very slow process. Since the polymers did not dissolve, the experiments had to be abandoned.

In the following, the results from the ABA type copolymers, P[$(MOx)_{20}$-$(NOx)_7(MOx)_{14}$] and P[$(MOx)_{30}(NOx)_7(MOx)_{26}$], will be described.

Determination of CMC

To determine the CMC, the same strategy as for the diblock copolymers was applied: Labeled polymers were used as tracers in solutions of the identical non-labeled polymers, in order to cover a larger concentration range. The

solutions were heated to 80°C for more than 12 hours in order to suppress non-equilibrium aggregates, and indeed, no non-equilibrium aggregates could be detected with FCS on these annealed samples.

Figure 3.18 shows FCS correlation curves of $P[(MOx)_{30}(NOx)_7(MOx)_{26}]$ having polymer concentrations in the range 7×10^{-9}-4×10^{-4} M. The behavior is very similar to the one of the diblock copolymers: Below the CMC, only one diffusion process is observed, which corresponds to the labeled unimers. Above the CMC, an additional slower, diffusional decay can be observed, which is due to micelles. The higher the concentration, the more pronounced

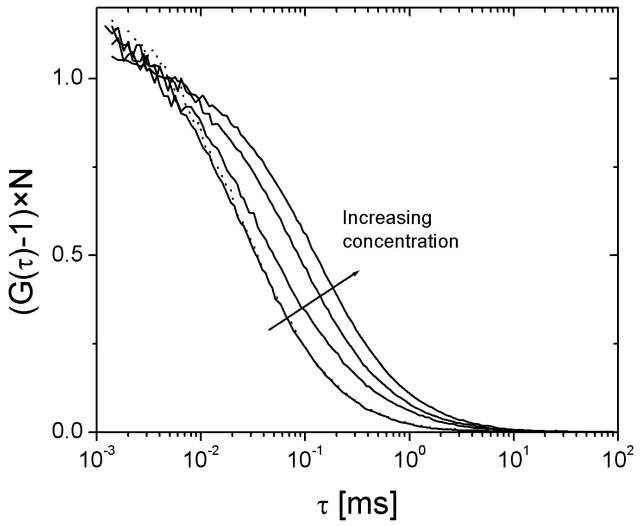

Figure 3.18 FCS correlation functions from solutions of $P[(MOx)_{30}(NOx)_7$-$(MOx)_{26}]$. The lowest concentration (7×10^{-9} M) is a solution of labeled polymers only (dotted line), whereas the other concentrations (8×10^{-7}, 8×10^{-6}, 8×10^{-5} and 4×10^{-3} M) are solutions containing both labeled and non-labeled polymers with the concentration of the labeled polymers being 7×10^{-9} M.

is the slow diffusional process, because the fraction of micelles increases with increasing concentration, as observed with the diblock copolymers (section 3.2.2). This was observed for the other triblock copolymer as well.

The concentration dependence of the diffusion coefficients of the triblock copolymers $P[(MOx)_{20}(NOx)_7(MOx)_{14}]$ and $P[(MOx)_{30}(NOx)_7(MOx)_{26}]$ is shown in figure 3.19. They look similar to the results from the diblock copolymers (figure 3.13). The CMC's are found at $(3 \pm 2) \times 10^{-6}$ M and

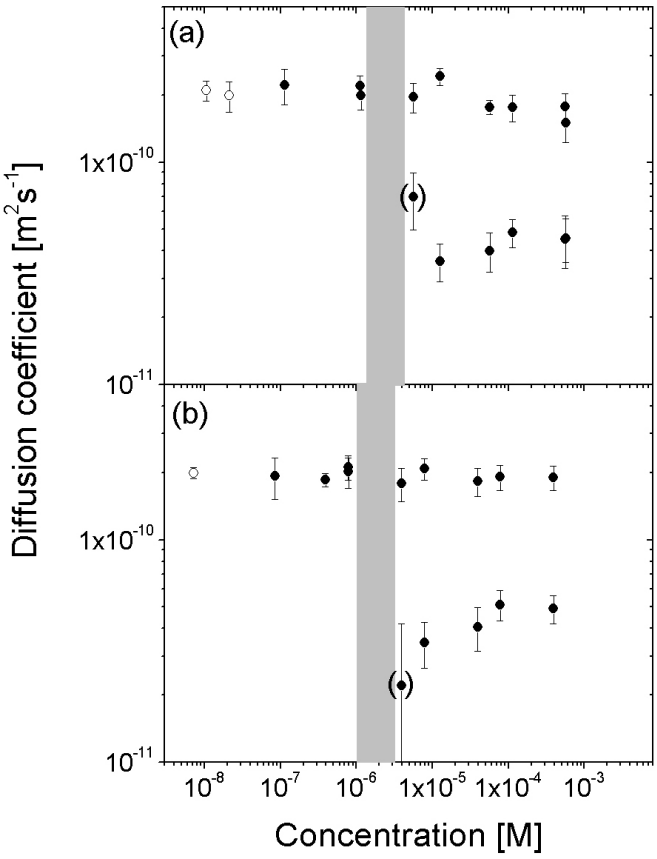

Figure 3.19 The concentration dependence of the diffusion coefficients of $P[(MOx)_{20}(NOx)_7(MOx)_{14}]$ (a) and $P[(MOx)_{30}(NOx)_7(MOx)_{26}]$ from FCS. Open symbols are from measurements on solutions containing labeled polymers only, whereas closed symbols are from solutions containing both labeled and non-labeled polymers. The gray bars indicates the CMC. The uncertainties are determined from repeated measurements (at least five). The data points in parentheses were not considered for the calculation of the average diffusion coefficients.

$(2 \pm 1) \times 10^{-6}$ M for $P[(MOx)_{20}(NOx)_7(MOx)_{14}]$ and $P[(MOx)_{30}(NOx)_7$-$(MOx)_{26}]$, respectively. These values are very similar to each other, even though the degree of polymerization of the hydrophilic blocks are different. It has been found with di- and triblock copolymers of ethylene oxide and propylene oxide, that the length of the hydrophilic block has little or no influence on the CMC [105, 106, 107]. This is in good agreement with our

Table 3.4 The hydrodynamic radii of the unimers ($r_{H,unimer}$), hydrodynamic radius of the micelles ($r_{H,micelles}$) and CMC's of the triblock copolymers, as determined by FCS. The values for the hydrodynamic radii are the average values from figure 3.19. For the micellar hydrodynamic radius, the lowest concentrations above the CMC, have been disregarded due to the high uncertainty.

	$P[(MOx)_{20}(NOx)_7(MOx)_{14}]$	$P[(MOx)_{30}(NOx)_7(MOx)_{26}]$
r_H^{unimer}	1.3 ± 0.3 nm	1.4 ± 0.2 nm
$r_H^{micelles}$	5.7 ± 0.7 nm	5.6 ± 0.9 nm
CMC	$(3 \pm 2)\times10^{-6}$ M	$(2 \pm 1)\times10^{-6}$ M

results.

The average unimer and micellar diffusion coefficients of $P[(MOx)_{20}(NOx)_7(MOx)_{14}]$ are $(1.9\pm0.2)\times10^{-10}$ m^2s^{-1} and $(4.3\pm0.5)\times10^{-11}$ m^2s^{-1}, which corresponds to hydrodynamic radii of 1.3±0.3 nm for the unimers and 5.7±0.7 nm for the micelles.

Very similar behavior is observed for the triblock copolymer with the longer P(MOx) blocks, $P[(MOx)_{30}(NOx)_7(MOx)_{26}]$. The diffusion coefficients for the labeled unimers and micelles are $(1.8 \pm 0.4)\times10^{-10}$ m^2s^{-1} and $(4.4 \pm 0.7)\times10^{-11}$ m^2s^{-1}, which corresponds to hydrodynamic radii of 1.4 ± 0.2 nm and 5.6 ± 0.9 nm for the unimers and micelles, respectively.

The hydrodynamic radii and the CMC-values are compiled in table 3.4. The hydrodynamic radius of the labeled unimers, $r_H^{unimers}$, for the two triblock copolymers are very similar, though it might be expected, that the hydrodynamic radius of $P[(MOx)_{30}(NOx)_7(MOx)_{26}]$ is larger than the one of $P[(MOx)_{20}(NOx)_7(MOx)_{14}]$, because of the higher degree of polymerization of the P(MOx) blocks. If the scaling behavior of the triblock copolymers is the same as for the homopolymers, labeled unimers of $P[(MOx)_{30}(NOx)_7(MOx)_{26}]$ should have a hydrodynamic radius of $r_H = 1.5$ nm, when compared with $P[(MOx)_{20}(NOx)_7(MOx)_{14}]$ (using equation 3.2 with $\nu = 0.36$). The hydrodynamic radius of the labeled unimers of $P[(MOx)_{20}(NOx)_7(MOx)_{14}]$ is comparable with the value of $P(MOx)_{45}$ ($r_H = 1.4 \pm 0.1$ nm). The hydrodynamic radius of the labeled unimers of $P[(MOx)_{30}(NOx)_7(MOx)_{26}]$ is comparable to that of $PMOx_{60}$ ($r_H = 1.5\pm0.1$ nm).

The hydrodynamic radii of the micelles are found to be 5.7±0.7 nm and 5.6±0.9 nm for $P[(MOx)_{20}(NOx)_7(MOx)_{14}]$ and $P[(MOx)_{30}(NOx)_7(MOx)_{26}]$, respectively. This is contradictory to the expectation, that the micellar hydrodynamic radius increases with the degree of polymerization.

Previously, an increase in the hydrodynamic radius of micelles with the degree of polymerization has been reported. Narrainen et al. determined the hydrodynamic radius of two triblock copolymers of different degree of polymerization in aqueous solution [108], having poly(*n*-butyl methacrylate) (BMA) as the hydrophobic and poly[(2-dimethylamino)ethyl methacrylate] (DEM) as the hydrophilic block, respectively, of the following compositions $P[(DEM)_{49}(BMA)_{58}(DEM)_{49}]$ and $P[(DEM)_{92}(BMA)_{58}(DEM)_{92}]$. The hydrodynamic radii are 32.3 and 65.2 nm, respectively. Their results thus indicate that the micellar hydrodynamic radius is proportional to the degree of polymerization.

A linear relation between the micellar hydrodynamic radius and the degree of polymerization of the hydrophilic block, was also found in aqueous solutions of triblock copolymers of the BAB type, composed of hydrophobic oxybutylene (OB) and hydrophilic oxyethylene (OE) [109]. The hydrodynamic radius for the polymer with lowest degree of polymerization, $P[(OB)_7(EO)_{22}(OB)_7]$, was $\sim$ 5 nm and for the highest degree of polymerization, $P[(OB)_{10}(EO)_{271}(OB)_{10}]$, $\sim$ 13 nm. The authors anticipate the same behavior for ABA-type triblock copolymers.

These results indicate that, in our study, the range of the degree of polymerization of the hydrophilic block was not large enough to observe the expected increase in micellar hydrodynamic radius.

3.3.2 Random copolymer

The random copolymer is different from the previously described block copolymers in that the hydrophobic and hydrophilic monomers are not arranged in blocks, but are randomly distributed along the polymer backbone.

First a random copolymer with the composition $P[(MOx)_{33}(NOx)_{11}]_{random}$ was supplied, which however, did not dissolve in water, probably because the content of NOx monomers was too high. Therefore a new random copolymer was supplied, $P[(MOx)_{40}(NOx)_6]_{random}$, which has a lower hydrophobic content and it was possible to dissolve this polymer in water. Again, the CMC was determined from the concentration dependence of the diffusion coefficients measured with FCS and the micellar size was characterized. As before, fluorescence labeled polymers are used as tracers in solutions of the identical non-labeled polymers.

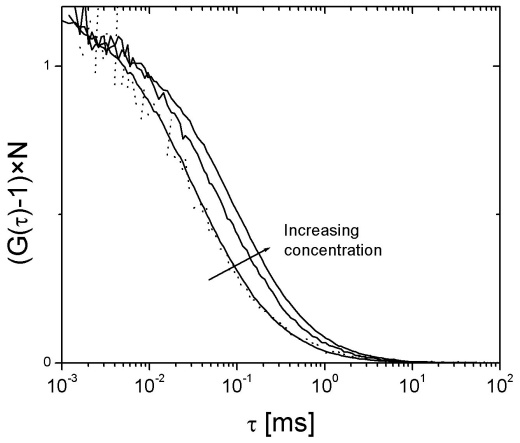

Figure 3.20 FCS correlation functions measured at four different concentrations. The lowest concentration was a solution with only labeled polymers, at a concentration of 3×10^{-8} M (dashed line). The other curves are from solutions containing both labeled and non-labeled polymers. The concentration of the labeled polymers is in the range of 1-3×10^{-8}M. The concentrations of non-labeled polymers are 5.3×10^{-6} M, 1.1×10^{-4} M and 1.7×10^{-3} M.

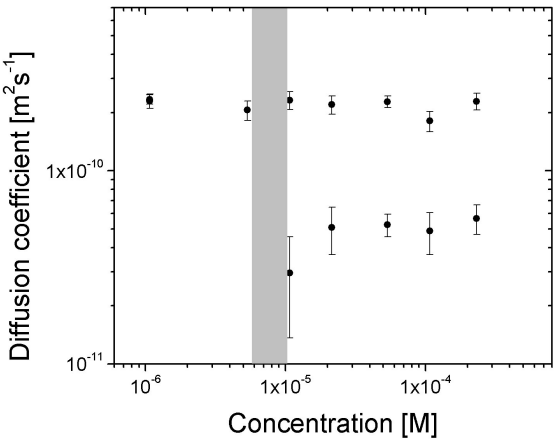

Figure 3.21 The concentration dependence of the diffusion coefficient for $P[(MOx)_{40}(NOx)_6]_{random}$. The gray bar indicates the CMC. The graph shows measurements done on solutions of both labeled and non-labeled polymers.

Determination of the CMC

Figure 3.20 shows four FCS correlation curves from solutions of annealed $P[(MOx)_{40}(NOx)_6]_{random}$. In solutions of labeled polymers at low concentrations (3×10^{-8} M), only one diffusional decay is observed, having a diffusion coefficient $(2.1\pm0.2)\times10^{-10}$ m^2s^{-1}, which corresponds to a hydrodynamic radius of 1.2±0.1 nm (table 3.5). The hydrodynamic radius of the random copolymer is lower than the one of the $P(MOx)_{45}$ homopolymer (1.4 ± 0.1 nm), which points to a more compact conformation of the random copolymer. This is possible caused by shielding of the hydrophobic P(NOx) monomers from the water. This was not the case with the diblock and triblock copolymers described above.

At higher polymer concentrations, an additional slower diffusional decay was observed. Its amplitude increases with concentration, just as with the di- and triblock copolymers. The concentration dependence of the diffusion coefficient is shown in figure 3.21. The average diffusion coefficient of the micelles is $(5.2 \pm 0.3) \times 10^{-11}$ m^2s^{-1}, which corresponds to a hydrodynamic radius of 4.7 ± 0.3 nm.

Table 3.5 The hydrodynamic radius of the unimers (r_H^{unimer}), and the micelles ($r_H^{micelles}$) and CMC, for $P[(MOx)_{40}(NOx)_6]_{random}$as determined by FCS. The lowest concentration above CMC, is not included in the average of $r_H^{micelle}$, because of the high uncertainty.

	$P[(MOx)_{40}(NOx)_6]_{random}$
r_H^{unimer}	1.2±0.1 nm
$r_H^{micelle}$	4.7±0.3 nm
CMC	$(8 \pm 3)\times10^{-6}$ M

The hydrodynamic radius of the micelles is comparable with the hydrodynamic radius of the micelles of the triblock copolymers. However, the random copolymer is not expected to form core-shell micelles with P(NOx) in the core like with block copolymers, because the hydrophobic and hydrophilic monomers are not arranged in separate blocks. One possible structure could be that only the hydrophobic nonyl side-chains form the micellar core with the polymer backbone at the surface, as sketched in figure 3.22b. An estimate of the length of the nonyl side-chains [60], however, gives only ~1.0-1.2 nm, which is roughly half the length of the hydrophobic block of $P[(MOx)_{40}$-$(NOx)_7]$. This shows, that the structure of the micelles is not as simple as

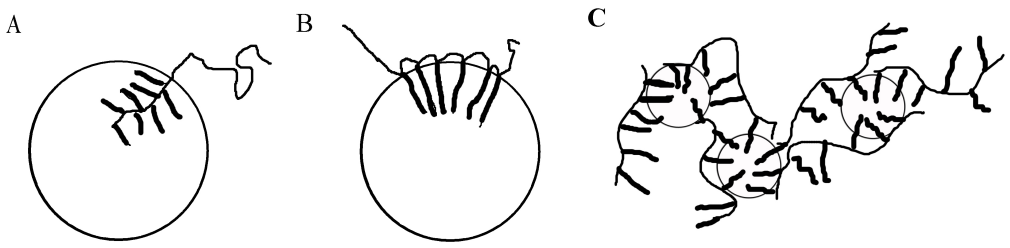

Figure 3.22 Sketch of three P[(MOx)(NOx)] micelle structures: A micelle from diblock copolymers, where the micellar core is formed by the hydrophobic block (A). A possible structure of a micelle from random copolymers, where the micelle core consists of the nonyl side chains (B). Another possible structure of a micelle from random copolymers, which contains more, but smaller, hydrophobic domains (C).

sketched in figure 3.22B, since this would result in a smaller micellar radius. One possibility could be that the micelle contains several hydrophobic domains which are irregularly distributed and which are connected by the polymer backbone and the (MOx) monomers, see figure 3.22C. Such a structure was observed by Sato et al. [17] with random copolymers of acrylic acid and N-dodecylmethacrylamide for a hydrophobic content of the polymer above ~22 mol% and concentrations above 20 g/L ($\sim 10^{-3}$ M).

The CMC was determined to be $(8 \pm 3)\times10^{-6}$ M. Sato et al determined a CMC of 8×10^{-7} M at a molar mass of ~9000 g mole^{-1}, for the polymer system described above [17]. Noda et al. investigated random copolymers of sodium 2-(acrylamido)2-methylpropanesulfonate and dodecyl methacrylate (with a molar mass of 42.000 g mole^{-1} and the hydrophobic part having 9 mole% of the polymer. They determined a CMC of 9×10^{-7} M, using steady state fluorescence [110]. The CMC of the random copolymer measured by us with $P[(MOx)_{40}(NOx)_6]_{random}$ is of the same order.

3.3.3 Summary

In addition to the diblock copolymers we have studied the CMC and the hydrodynamic radii of two triblock copolymers and a random copolymer.

The triblock copolymers had the same degree of polymerization of the hydrophobic block, but the degree of polymerization of the hydrophilic block was varied. Neither the hydrodynamic radius nor the CMC were affected by

this variation, probably because the difference in degree of polymerization was not large enough.

With the random copolymer, the hydrodynamic radius of the unimers was lower than the ones of the other block copolymers, which could indicate a more compact structure. The micellar hydrodynamic radius was also smaller. This is probably due to the structure of the aggregates which are not expected to be core-shell micelles for the random copolymer.

3.4 Comparison of the polymer systems

In this section, the effect of the polymer architecture on the hydrodynamic radius of the unimers, the size and structure of the micelles and the CMC are discussed.

3.4.1 Unimer size

The hydrodynamic radii of four homopolymers of different degree of polymerization, two diblock copolymers with the fluorescence dye attached at different positions, two triblock copolymers with different degrees of polymerization of the hydrophilic blocks (the degree of polymerization of the hydrophobic block was kept constant) and one random copolymer are compiled in figure 3.23. The hydrodynamic radius of the fluorescence dye TRITC,

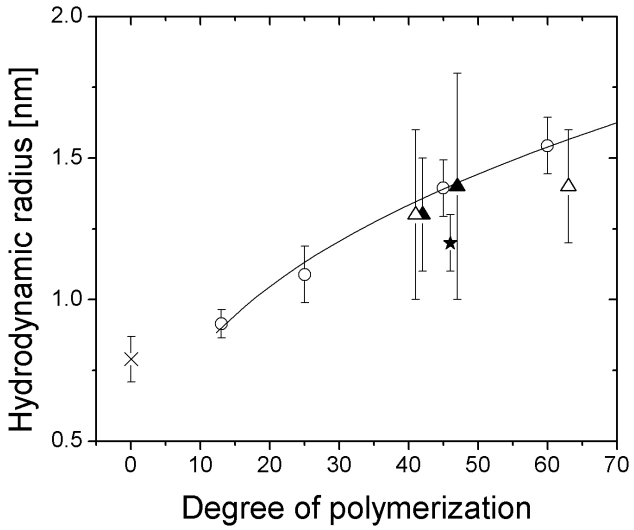

Figure 3.23 The hydrodynamic radius as a function of the overall degree of polymerization for the different polymers: TRITC (×, degree of polymerization zero), homopolymers (○), diblock copolymers (▲), triblock copolymers (△) and random copolymer (⋆). The line is identical to the one in figure 3.4 assuming a coil conformation, and serves as a guide to the eye.

which was used to label all the polymers, is shown as a reference (corresponding to a degree of polymerization of zero).

The hydrodynamic radius increases with the degree of polymerization of the homopolymers, as expected (see section 3.1.2). A change in architecture to diblock or triblock copolymers, i.e. replacing a fraction of the P(MOx) by P(NOx) groups, does not have an effect on the unimer size.

In contrast, the hydrodynamic radius of the random copolymer is significantly lower than the one of a homopolymer with similar degree of polymerization. This indicates a more compact structure of the unimers of the random copolymer, probably due to the shielding of the hydrophobic side-chains from the water, resulting in a lower hydrodynamic radius.

3.4.2 The micellar size

All copolymers are found to form aggregates above a certain concentration, the CMC. The resulting average hydrodynamic radii are compiled in table 3.6.

Table 3.6 Hydrodynamic radius of the copolymer micelles as determined using FCS.

Polymer	$r_{H,micelle}$ [nm]
$P[(MOx)_{40}(NOx)_7]$	13±2
$P[(NOx)_{10}(MOx)_{32}]$	11.3±0.9
$P[(MOx)_{20}(NOx)_7(MOx)_{14}]$	5.6±0.7
$P[(MOx)_{30}(NOx)_7(MOx)_{26}]$	5.6±0.9
$P[(MOx)_{40}(NOx)_6]_{random}$	4.7±0.3

As seen in table 3.6, the hydrodynamic radii of the micelles from the triblock copolymers are smaller than the hydrodynamic radii of the diblock copolymers. This has previously been observed with copolymers of ethylene oxide and propylene oxide in aqueous solution, when the degree of polymerization is similar [41].

The diblock copolymer micelles are larger than the triblock copolymer micelles, which may be related to the difference in architecture since the degrees of polymerization are comparable. The difference between the hydrodynamic radius of the diblock and triblock copolymer micelles is a factor of two. The expected architecture of the micelles formed by diblock and triblock copolymers is sketched in figure 3.24.

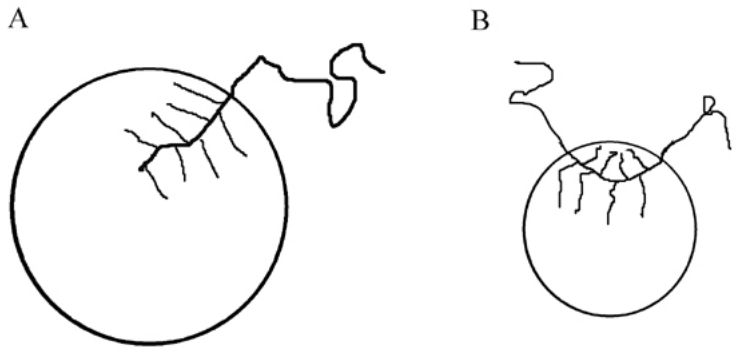

Figure 3.24 Architecture of micelles formed by diblock copolymers (A) and triblock copolymers (B), respectively. The circles indicate the hydrophobic part (micellar core).

The diblock copolymer has only one junction that must be located at the interface between the micelle core and the corona, whereas the triblock copolymer has two. For the diblock copolymer, the core radius can be as large as the length of the hydrophobic block (if completely stretched blocks are assumed), whereas for the triblock polymers, the radius is closer to half the length of the hydrophobic block. Therefore, the maximum possible radius of spherical micelles from a diblock copolymer is twice the one of micelles from triblock copolymers.

The hydrodynamic radius of the micelles formed by the random copolymer is smaller than the ones of the block copolymers. The random copolymer aggregates most probably have a different structure from the di- and triblock copolymer micelles.

3.4.3 The critical micelle concentration

The CMC of the diblock copolymers was determined by FCS on solutions with a small concentration of the labeled copolymers and varying the concentration of non-labeled polymers. In section 3.2.3, it was established that the observations on the labeled copolymers cannot be described by the closed-association model for aggregation, which points to a coupled equilibrium between the labeled polymers the micelles consisting of non-labeled polymers. This indicates, that the aggregation behavior of labeled and non-labeled polymers is not the same and the CMC taken as the onset of the appearance of the labeled micelles is not necessarily correct. If the concentration of non-

labeled micelles has to be relative high before the labeled polymers attach to them, the CMC is overestimated. Since it is not straightforward to verify the low CMC's with other methods, an additional FCS measurement was made using another tracer (the fluorescence dye rhodamine 6G). The such determined CMC was the same. This means that two significantly different tracers lead to the same CMC, even though the non-polymeric tracer is more loosely attached to the micelles than the polymeric tracer. This observation indicate that the FCS results are reliable.

The CMC's determined with FCS are collected in table 3.7.

Table 3.7 The CMC's from the different copolymers determined using FCS.

Polymer	CMC [10^{-6} M]
P[$(MOx)_{40}(NOx)_7$]	8 ± 2
P[$(NOx)_{10}(MOx)_{32}$]	20 ± 10
P[$(MOx)_{20}(NOx)_7(MOx)_{14}$]	3 ± 2
P[$(MOx)_{30}(NOx)_7(MOx)_{26}$]	2 ± 1
P[$(MOx)_{40}(NOx)_6$]$_{random}$	8 ± 3

The CMC of the random copolymer is 8×10^{-6} M, which is comparable to that of the diblock copolymers. This is likely because the degree of polymerization of the hydrophobic block is comparable.

The CMC's of the triblock copolymers are lower than the ones of the diblock copolymer, even though their hydrophobic blocks have the same degree of polymerization. Often it has been observed that the CMC's of triblock copolymers are higher or equal to the CMC of diblock copolymers with the same chemical composition. The reason is that the triblock copolymers have two junction points in the interface between the core and the corona, whereas the diblock copolymers have only one [41] (see figure 3.24). For instance, in aqueous solutions of poly(ethylene oxide)-poly(propylene oxide) based block copolymers the CMC determined using static light scattering and surface tension was higher for triblock copolymers than for diblock copolymers of similar composition [41]. Also for aqueous solutions of poly(oxy ethylene)-poly(oxy butylene), the CMC determined with surface tension, the CMC's for the triblock copolymers were at a higher concentration than for the diblock copolymers with similar composition [42]. Narrainen et al. determined the CMC of poly(n-butyl methacrylate)-poly[(2-dimethylamino)ethyl methacrylate] based di- and triblock copolymers in aqueous solutions, using fluorescence measurements with pyrene as fluorescence probe. They found

that the CMC of the di- and triblock copolymers were identical [108]. One explanation why our triblock copolymers have lower CMC's than the diblock copolymers may be the preparation of the solutions. The diblock copolymer solutions were filtered and annealed during the PCS measurements. If some polymers have been left in the filter, this would mean that the CMC's of the diblock copolymers are overestimated.

4 Conclusion

The diffusion coefficient of different architectures of fluorescence labeled oxazoline based polymers has been investigated. Using FCS, the diffusion coefficient of four different polymer architectures was measured. The polymer architectures were homopolymers, diblock copolymers, triblock copolymers and a random copolymer.

The diffusion coefficients of the homopolymers were measured as a function of concentration and degree of polymerization. For concentrations above $\sim 10^{-4}$ M, the diffusion coefficient was observed to decrease, however at lower concentrations, the diffusion coefficient was constant and corresponded to the diffusion coefficient at nominal zero concentration, D_0. As the degree of polymerization was increased, the diffusion coefficient was observed to decrease. The functionality was modelled by assuming coil or rod-like particles. None of these models described the experimental data satisfactorily, probably due to the influence of the fluorescence dye.

The concentration dependence of the diffusion coefficient of the diblock copolymers was measured. First experiments showed that when the polymers were dissolved in water at room temperature, large non-equilibrium aggregates were detected together with both labeled unimers and equilibrium micelles. After the solutions were annealed by heating only labeled unimers and equilibrium micelles were detected with FCS. The coexistence of non-equilibrium aggregates and equilibrium micelles, as well as the effect of annealing, was also observed by both PCS and SANS. From the concentration dependence of the diffusion coefficient the low CMC ($\sim 10^{-5}$ M) could be determined. The micellar hydrodynamic radius corresponded to the value determined by PCS. Positioning the fluorescence dye at the hydrophobic or the hydrophilic part of the polymer, did not influence neither the hydrodynamic radii nor the CMC of the diblock copolymers in aqueous solution. The aggregation behavior was modelled by the closed-association model. This model did not give a good description of the aggregation behavior. This is probably because the fluorescence dye alters the aggregation behavior of the single polymer. The CMC was also determined with FCS

using a low molar mass tracer instead of a polymeric tracer. The two tracers gave the same CMC. The micellar hydrodynamic radius determined with the low molar mass tracer was lower than those obtained using the polymeric tracer, which indicates the advantage of using polymeric tracers in FCS experiments.

The CMC as well as the hydrodynamic radii of two triblock copolymers and a random copolymer was determined by the same strategy as for the diblock copolymers. The CMC's of the triblock copolymers were lower than those for the diblock copolymers, whereas for the random copolymer the CMC was comparable with the diblock copolymers. The micellar hydrodynamic radii of the triblock copolymers were approximately half of the micellar hydrodynamic radius of the triblock copolymers, which is expected from the structure of the formed micelles.

Oxazoline-based polymers proved to be a versatile system, where a stable fluorescence labeling made it possible to perform FCS measurements. By labeling the polymers, it is possible to produce a tracer for the FCS experiments, which closely resembles the polymers. A wide range in polymer concentration is thereby possible by using solutions of labeled and non-labeled polymers.

FCS proved to be an efficient method to study the aggregation behavior of fluorescence labeled polymers. The method is fast and allows measurements at much lower concentrations than many other traditionally used methods. The low measurement time allows studies of reaction kinetics, that take place in the time range of minutes to hours and where the diffusion coefficient is altered by the reaction. Furthermore it opens for the possibility to investigate the behavior of single molecules in concentrated solutions or gels.

Bibliography

[1] D. F. Evans and H. Wennerström. *The Colloidal Domain.* Wiley-VCH. New york, 2 edition, 1999.

[2] M. Eigen. *Biophys. Chem.*, 63:A1, 1996.

[3] M. Fändrich, M. A. Fletcher, and C. M. Dobson. *Nature*, 410:165, 2001.

[4] P. Alexandridis and T. A. Hatton. Block copolymer micelles (overview). In J. C. Salamone, editor, *Polymeric Materials Encyclopedia*, page 743. CRC Press, Baco Raton, 1996.

[5] A. Halperin. *Macromolecules*, 20:2943, 1987.

[6] P. Linse and M. Björling. *Macromolecules*, 24:6700, 1991.

[7] K. Mortensen. *J. Phys. Condens. Matter*, 8:A103, 1996.

[8] I. W. Hamley. *The Physics of Block Copolymers.* Oxford University Press, Oxford, 1998.

[9] N. S. Cameron, M. K. Corbierre, and A. Eisenberg. *Can. J. Chem.*, 77:1311, 1999.

[10] W. Brown and K. Mortensen, editors. *Scattering in Polymeric and Colloidal Systems.* Gordon and Breach Science Publishers, Amsterdam, 2000.

[11] P. Alexandridis and B. Lindman, editors. *Amphiphilic Block Copolymers: Self-Assembly and Applications.* Elsevier, Amsterdam, 2000.

[12] A. Choucair and A. Eisenberg. *Eur. Phys. J. E.*, 10:37, 2003.

[13] P. Munk. *Introduction to Macromolecular Science.* John Wiley & Sons, Inc., 1989.

[14] M. Nguyen-Misra and W. L. Mattice. *Macromolecules*, 28:144, 1995.

[15] D. Lairez, M. Adam, J.-P. Carton, and E. Raspaud. *Macromolecules*, 30:6798, 1997.

[16] G. Fleischer, Č. Koňák, A. Puhlmann, F. Rittig, and J. Kärger. *Macromolecules*, 33:7066, 2000.

[17] Y. Sato, A. Hashidzume, and Y. Morishima. *Macromolecules*, 34:6121, 2001.

[18] P. N. Hurter and T. A. Hatton. *Langmuir*, 8:1291, 1992.

[19] G. S. Kwon and K. Kataoka. *Adv. Drug Delivery Rev.*, 16:295, 1995.

[20] A. V. Kabanov and V. A. Kabanov. *Adv. Drug Delivery Rev.*, 30:49, 1998.

[21] C. Allen, D. Maysinger, and A. Eisenberg. *Colloids Surf. B.*, 16:3, 1999.

[22] S. N. Sidorov, L. M. Bronstein, P. M. Valetsky, J. Hartmann, H. Colfen, H. Schnablegger, and M. Antonietti. *Colloid Interface Sci.*, 212:197, 1999.

[23] D. M. Chernysov, L. M. Bronstein, H. Borner, B. Berton, and M. Antonietti. *Chem. Mater.*, 12:114, 2000.

[24] G. Wanka, H. Hoffmann, and W. Ulbricht. *Macromolecules*, 27:4145, 1994.

[25] D. F. Sigueira and S. P. Nunes. *Polymer*, 35:490, 1994.

[26] K. Mortensen and J. S. Pedersen. *Macromolecules*, 26:805, 1993.

[27] O. Glatter, G. Scherf, K. Schillén, and W. Brown. *Macromolecules*, 27:6046, 1994.

[28] M. Almgren, W. Brown, and S. Hvidt. *Colloid Polym. Sci.*, 273:2, 1995.

[29] Z. Tuzar and P. Kratochvíl. Micelles of block and graft copolymers in solutions. In E. Matijević, editor, *Surface and Colloid Science*, page 1. Plenum Press, New York, 1993.

[30] Z. Tuzar and P. Kratochvíl. Scattering from block copolymer micellar systems. In W. Brown, editor, *Light Scattering: Principles and Development*. Oxford Science Publications, New York, 1996.

[31] G. Fleischer. *J. Phys. Chem.*, 97:517, 1993.

[32] G. Fleischer, P. Bloß, and W.-D. Hergeth. *Colloid Polym. Sci.*, 271:217, 1993.

[33] S. Hvidt, E. B. Jørgensen, W. Brown, and K. Schillén. *J. Phys. Chem.*, 98:12430, 1994.

[34] B. Nyström and H. Walderhaug. *J. Phys. Chem.*, 100:5433, 1996.

[35] G. Riess. *Prog. Polym. Sci.*, 28:1107, 2003.

[36] B. V. Lent and J. M. H. M. Scheutjens. *Macromolecules*, 22:1931, 1989.

[37] P. Linse. *Macromolecules*, 26:4437, 1993.

[38] M. Malmsten, P. Linse, and K.-W. Zhang. *Macromolecules*, 26:2905, 1993.

[39] P. Munk. Equilibrium and nonequilibrium polymer micelles. In S. E. Webber, P. Munk, and Z. Tuzar, editors, *Solvents and Self-Organization of Polymers*, volume 327 of *NATO ASI Series, Serie E: Applied Sciences*, page 19. Kluwer Academic Publishers, Dordrecht, 1996.

[40] H. Altinok, S. K. Nixon, P. A. Gorry, D. Attwood, C. Booth, A. Kelarakis, and C. Havredaki. *Coll. Surf. B*, 16:73, 1999.

[41] H. Altinok, G.-E. Yu, K. Nixon, P. A. Gorry, D. Attwood, and C. Booth. *Langmuir*, 13:5837, 1997.

[42] S. S. Soni, N. V. Sastry, A. K. Patra, J. V. Joshi, and P. S. Goyal. *J. Phys. Chem. B.*, 106:13069, 2002.

[43] I. Astafieva, X. F. Zhong, and A. Eisenberg. *Macromolecules*, 26:7339, 1993.

[44] N. Kang, M.-E. Perron, R. E. Prud'homme, Y. Zhang, G. Gaucher, and J.-C. Leroux. *Nano Lett.*, 5:315, 2005.

[45] H. Schuch, J. Klingler, P. Rossmanith, T. Frechen, M. Gerst, J. Feldthusen, and A. H. E. Müller. *Macromolecules*, 33:1734–1740, 2000.

[46] K. Procházka, Z. Limpouchová, and S. E. Webber. Block copolymers micelles 2. fluorimetric studies and computer modeling. In J. C. Salamone, editor, *Polymeric Materials Encyclopedia*, page 764. CRC Press, Boca Raton, 1996.

[47] R. Erhardt, A. Böker, H. Zettl, H. Kaya, W. Pyckhout-Hintzen, G. Krausch, V. Abetz, and A. H. E. Müller. *Macromolecules*, 34:1069, 2001.

[48] K. Loos, A. Böker, H. Zettl, M. Zhang, G. Krausch, and A. H. E. Müller. *Macromolecules*, 38:873, 2005.

[49] M. A. Hink, A. Van Hoek, and A. J. W. G. Visser. *Langmuir*, 15:992, 1999.

[50] M. Litt, F. Rahl, and L. G. Roldan. *J. Polym. Sci. A-2*, 7:463, 1969.

[51] S. Kobayashi. *Prog. Polym. Sci.*, 15:752, 1990.

[52] K. Aoi and M. Okada. *Prog. Polym. Sci.*, 21:151, 1996.

[53] R. Jordan, K. Martin, H. J. Räder, and K. K. Unger. *Macromolecules*, 38:8858, 2001.

[54] M. C. Woodle, C. M. Engbers, and S. Zalipsky. *Bioconjugate Chem.*, 5:493, 1994.

[55] S. C. Lee, C. Kim, I. C. Kwon, H. Chung, and S. Y. Jeong. *journal of Controlled Release*, 89:437, 2003.

[56] O. Purrucker, A. Förtig, R. Jordan, and M. Tanaka. *ChemPhysChem*, 5:327, 2004.

[57] K. Lüdtke, R. Jordan, P. Hommes, O. Nuyken, and C. A. Neumann. *Macromol. Biosci.*, 5:384, 2005.

[58] P. Persigehl, R. Jordan, and O. Nuyken. *Macromolecules*, 33:6977, 2000.

[59] The handbook - a guide to fluorescent probes and labeling technologies. Molecular Probes. http://probes.invitrogen.com/handbook.

[60] Estimated using CS Chem 3D ultra 7.0.0.

[61] D. Magde, E. L. Elson, and W. W. Webb. *Phys. Rev. Lett.*, 29:705, 1972.

[62] E. L. Elson and D. Magde. *Biopolymers*, 13:1, 1974.

[63] D. Magde, E. L. Elson, and W. W. Webb. *Biopolymers*, 13:29, 1974.

[64] J. Widengren and Ü. Mets. Conceptual basis of fluorescence correlation spectroscopy and related techniques as tools in bioscience. In Ch. Zander, J. Enderlein, and R. A. Keller, editors, *Single Molecule Detection in Solution*. Wiley-VCH, Berlin, 2002.

[65] R. Rigler, Ü. Mets, J. Widengren, and P. Kask. *Eur. Biophys. J.*, 22:169, 1993.

[66] R. Rigler and E. Elson, editors. *Fluorescence Correlation Spectroscopy. Theory and Applications*. Springer, Berlin Heidelberg New York, 2000.

[67] P. Schwille and E. Haustein. *Fluorescence Correlation Spectroscopy: An Introduction to its Concepts and Applications*. Biophysics Textbook Online (BTOL), http://www.biophysics.org/education/techniques.htm, 2002.

[68] Carl Zeiss Advanced Imaging Microscopy, Jena, Germany. *LSM 510 - Confocor 2 Applications Manual*, 2001.

[69] S. R. Aragon and E. Pecora. *J. Chem. Phys.*, 64:1791, 1976.

[70] A. G. Palmer and N. L. Thompson. *Biophys. J*, 51:339, 1987.

[71] J. Widengren, Ü. Mets, and R. Rigler. *J. Phys. Chem.*, 99:13368, 1995.

[72] A. Einstein. *Annalen der Physik*, 17:549, 1905.

[73] B. J. Berne and P. Pecora. *Annu. Rev. Phys. Chem.*, 25:233, 1974.

[74] W. Brown, editor. *Dynamic Light Scattering: The Method and some Applications*. Oxford University Press Inc., New York, 1993.

[75] P. Štěpánek. Data analysis in dynamic light scattering. In W. Brown, editor, *Dynamic Light Scattering: The Method and some Applications*, page 177. Oxford University Press Inc., New York, 1993.

[76] J. Jakeš. *Coll. Chem. Commun.*, 60:1781, 1995.

[77] http://www.fki.uu.se/robert.johnsen/gendist.htm.

[78] R. D. Mountain and J. M. Deutch. *J. Chem. Phys.*, 50:1103, 1972.

[79] H. Brumberger, editor. *Modern Aspects of Small-Angle Scattering*, NATO ASI Series, Dordrecht, 1995. Kluwer Academic Publishers.

[80] From the GKSS homepage, 2005:
http://www.gkss.de/templates/images_d/werkstoff/sans2_schematic.gif.

[81] K. Mortensen. Block copolymers studied with small angle neutron scattering. In W. Brown and K. Mortensen, editors, *Scattering in Polymeric and Colloidal Systems*, page 413. Gordon and Breach Science Publishers, Amsterdam, 2000.

[82] P. Biemann, M. Haese-Seiller, and P. Staron. *Physica B*, 276:156, 2000.

[83] F. P. Cheng, A. E. Ames, and L. D. Taylor. *Macromolecules*, 23:4688, 1990.

[84] H. Mays, K. Mortensen, and W. Brown. Microemulsions studied by scattering techniques. In W. Brown and K. Mortensen, editors, *Scattering in Polymeric and Colloidal Systems*, page 249. Gordon and Breach Science Publishers, Amsterdam, 2000.

[85] O. Glatter. Small-angle scattering and light scattering. In P. Lindner and T. Zemb, editors, *Neutron, X-Ray and Light Scattering: "Introduction to an Investigative Tool for Colloidal and Polymeric Systems"*, page 33. North-Holland, Amsterdam, 1991.

[86] O. Glatter. *J. Appl. Cryst.*, 10:415, 1977.

[87] A. Bergman, J. Brunner-Popele, G. Fritz, O. Glatter, R. Mittelbach, and B. Weyerich. *PCG Software Version 1.01.02.* Institut für Chemie, University of Graz, 2000.

[88] J. Brunner-Popela and O. Glatter. *J. Appl. Cryst.*, 30:431, 1997.

[89] M. Doi and S. F. Edwards. *The Theory of Polymer Dynamics.* International Series of Monographs on Physics. Oxford Science Publications, 1986.

[90] B. Dünweg, D. Reith, M. Steinhauser, and K. Kremer. *J. Chem. Phys.*, 117:914, 2002.

[91] Robert C. Weast, editor. *Handbook of Chemistry and Physics.* The Chemical Rubber Co., Ohio, 48 edition, 1967-1968.

[92] S. A. Sukhishvili, Y. Chen, J. D. Müller, E. Gratton, K. S. Schweizer, and S. Granick. *Nature*, 406:146, 2000.

[93] J. Stejskal, Č. Koňák, M. Helmstedt, and P. Kratochvíl. *Collect. Czech. Chem. Commun.*, 58:2282, 1993.

[94] Z. Zhou, Y.-W. Yang, C. Booth, and B. Chu. *Macromolecules*, 29:8357, 1996.

[95] S. Dai, P. Ravi, C. Y. Leong, K. C. Tam, and L. H. Gan. *Langmuir*, 20:1597, 2004.

[96] W. Batsberg, S. Ndoni, C. Trandum, and S. Hvidt. *Macromolecules*, 37:2965, 2004.

[97] C. Qian, S. Grigoras, and L. D. Kennan. *Macromolecules*, 29:1260, 1996.

[98] V. Schädler, C. Nardig, U. Wiesner, and E. Mendes. *J. Phys. Chem. B*, 104:5049, 2000.

[99] R. Ivanova, T. B. Bonné, T. Komenda, K. Lüdtke, R. Jordan, and C. M. Papadakis. Multi-compartment micellar networks formed by lipophilic-hydrophilic-fluorophilic triblock copolymers in aqueous solution. Poster presented at the annual meeting of the Deutsche Physikalische Gesellschaft in Berlin, March 4-9, 2005.

[100] R. Innocenzi, H. Kozuka, and T. Yoko. *J. Non-cryst. Solids*, 201:26, 1996.

[101] J. Humpolíčková, K. Procházka, M. Hof, Z. Tuzar, and M. Špírková. *Langmuir*, 19:4111, 2003.

[102] R. Vogel, M. Harvey, G. Edwards, P. Meredith, Heckenberg, M. Trau, and H. Rubinsztein-Dunlop. *Macromolecules*, 35:2063, 2002.

[103] S. Hvidt. *Colloids and Surfaces A*, 112:201, 1995.

[104] N. P. Balsara, M. Tirrell, and T. P. Lodge. *Macromolecules*, 24:1975, 1991.

[105] P. Alexandridis, J. F. Holzwarth, and T. A. Hatton. *Macromolecules*, 27:2414, 1994.

[106] J. R. Lopes and W. Loh. *Langmuir*, 14:750, 1998.

[107] A. Kelaraks, Z. Yang, E. Pousia, S. K. Nixon, C. Price, C. Booth, I. W. Hamley, V. Castelletto, and J. Fundin. *Langmuir*, 17:8085, 2001.

[108] A. P. Narrainen, S. Pascual, and D. M. Haddleton. *J. Polym. Sci. A*, 40:439, 2002.

[109] T. Liu, Z. Zhou, C. Wu, V. M. Nae, and B. Chu. *Macromolecules*, 30:7624, 1997.

[110] T. Noda and Y. Morishima. *Macromolecules*, 32:4631, 1999.

A Symbols and abbreviations

Here is a list of the used symbols and abbreviations.

a	Monomer length
AF	Aminofluorescein
$A(\tau_r)$	Distribution of relaxation times
b	Effective bond length
b_i	Scattering length
B_i	Cubic b-spline functions used in GIFT software
$\langle C \rangle$	Average concentration
c	Concentration
C_i	Fourier transform of the Cubic b-spline functions used in GIFT software
c_t	Total polymer concentration
CMC	Critical Micelle Concentration
CMT	Critical Micelle Temperature
cts/s	Counts per second
d	Length of the fluorescence dye
d_i	Coefficient for B_i and C_i used in the GIFT program
D	Diffusion coefficient
D_0	Diffusion coefficient extrapolated to zero concentration
$f(q)$	Amplitude of neutron radiation at q
F	Triplet fraction
$F(t)$	Time dependent fluorescence signal
FCS	Fluorescence correlation spectroscopy
$g_2(\tau)$	Normalized PCS correlation function
g_i	Diffusional part of FCS correlation function
$G(\tau)$	FCS correlation
G'	Elastic modulus
$G_2(\tau)$	PCS correlation function
GIFT	Generalized Indirect Fourier Transformation
$I(q)$	Intensity as function of scattering angle
$I(t)$	Time dependent intensity

k	Number of different diffusing particles
K	Equilibrium constant
K_2	Equilibrium constant
k_B	Boltzmann's constant
K_g	Constant dependent on the SANS setup
L	Polymer length
L_c	Thickness of micelle coruna
$[M]$	Concentration of micelles
M_m	Molar mass of micelles
$\overline{M}_n$	Number average molar mass
$\overline{M}_w$	Weight average molar mass
n	Refractive index
N	Number of molecules in the detection volume
N_{agg}	Aggregation number
N_p	degree of polymerization
NMR	Nuclear magnetic resonance
$p\,(r)$	Pair distance distribution function
p_{mic}	Probability of finding the tracer attached to a micelle
PCS	Photon correlation spectroscopy
P(MOx)	Poly(2-methyl-2-oxazoline)
P(NOx)	Poly(2-*n*-nonyl-2-oxazoline)
q	Scattering vector
r	Distance
r_c	Core radius of micelles
r_g	Radius of gyration
r_H	Hydrodynamic radius
Rh6G	Rhodamine 6G
$r_H^{micelles}$	Hydrodynamic radius of micelles
$r_H^{unimers}$	Hydrodynamic radius of unimers
S^2	Structure factor (in FCS)
SANS	Small angle neutron scattering
SLS	Static light scattering
SSF	Steady state fluorescence
ST	Surface tension
T	Absolute temperature
T_E	Overall experimental time
THF	Tetrahydrofuran
TRITC	Tetramethyl rhodamine isothiocyanate
$[U]$	Concentration of unimers
V_{eff}	Effective volume

V_m	Molecular volume
w	Polymer width
w_o	Half width of the FCS detection volume
w_{NOX}	Number fraction of P(NOX)
z_0	Half height of the FCS detection volume
α	Fraction of polymers as micelles
η	Viscosity
η_s	Scattering length density fluctuations
γ	Instrumental constant in PCS
$\tilde{\gamma}$	Scattering length density correlation function
Γ	Relaxation rate
λ	Wavelength
ν	Exponent
Ω	Angular volume
ϕ	Fluorescence quantum yield
ρ_i	Amplitude of fluorescent species
ρ_s	Scattering length density
σ	Number of registered particles pr. unit time and incident flux
τ	Correlation time
τ_D	Diffusion time
τ_r	Relaxation time
τ_T	Triplet time
θ	Scattering angle

B Publications and presentations

B.1 Publications

T. B. Bonné, K. Lüdtke, R. Jordan, P. Štěpánek and C. M. Papadakis: "Aggregation behavior of amphiphilic poly(2-alkyl-2-oxazoline) diblock copolymers in aqueous solution studied by fluorescence correlation spectroscopy", **Colloid and polymer science** 282 (8): 833-843, 2004.

P. Busch, T. Bonné, D.-M. Smilgies, D. Posselt and C. M. Papadakis: "Kinetics studies of block copolymer thin films using small-angle x-ray scattering under grazing incidence (GISAXS)", **CHESS Newsletter**: 37-39, 2002.

B.2 Talk

Annual meeting of the German physical society: "Fluorescence Correlation Spectroscopy Investigations of Water-Soluble Polymers", 4-9 March 2005, Berlin, Germany.